Two Methods for Modeling Scalar Hysteresis and their use in Controlling Actuators with Hysteresis.

William S. Galinaitis

Dissertation submitted to the Faculty of the
Virginia Polytechnic Institute and State University
in partial fulfillment of the requirements for the degree of

Doctor of Philosophy
in
Mathematics

Robert C. Rogers, Chair
Daniel Inman
Werner Kohler
Joseph Ball
Robert Wheeler

November 30, 1999
Blacksburg, Virginia

Keywords: Hysteresis, Control, Preisach, Piezoelectric, Actuators

Two Methods for Modeling Scalar Hysteresis and their use in Controlling Actuators with Hysteresis.

by
William S. Galinaitis

(ABSTRACT)

The accurate control of a positioning system that exhibits scalar hysteresis requires a control strategy that incorporates compensation for the hysteresis. One approach is to develop a compensator based on an inverse hysteresis operator. This method uses an open loop control in which the inverse operation adjusts the actuator input to compensate for the hysteresis in the system. When this is accomplished, the composite operation produces a linear relationship between a reference input and the system output. The difficulty of this method lies in developing an accurate model of the hysteresis for which an inverse operator can be obtained.

In this work, a system with hysteresis is modeled by a generic model based on a Preisach type operator. First, it is shown that the operator has an inverse and that both have approximations that are convergent. Then, simulation and experimental data are used to demonstrate the ability of the operator to accurately model a hysteresis relationship. This lays the foundation for then demonstrating the concept of inverse compensation.

Acknowledgments

To my committee members, especially:

- Dr. R. Rogers for his mentorship;
- Dr. W. Kohler, who's funding supported this research under AFOSR AASERT Grant F49620 - 94 - 1 - 0350;
- Dr. D. Inman for access to the equipment necessary to perform the experimental work.

Special thanks to my wife, Diane, and my children, Alyssa and Ryan, for their support through it all.

I also wish to thank my parents and Diane's parents for all the support that they have given me and my family during this doctoral process:

Mr. and Mrs. William G. Galinaitis
and
Mr. and Mrs. George F. Muller

Thank you!

Contents

1 Overview **1**

2 Background **3**

2.1 Actuators and Scalar Hysteresis 3

2.2 The Positioning Problem 4

2.3 The Solution, Inverse Compensation 7

3 Preisach Operator P and the Inverse $\mathbf{P}^{-1}$ **9**

3.1 Description of the Preisach Operator $\mathbf{P}$ 9

3.1.1 The Preisach Operator Defined as a Composition. 18

3.2 $\mathbf{P^{-1}}$ 19

3.3 The Computational Formula for the Forward Model 21

3.4 Forward and Inverse Models using the Bivariate Density Function. 22

3.4.1 Computation of the Inverse 23

3.5 Simulation 24

4 The KP Operator $\mathbf{W}_{kp}$ and Inverse $\mathbf{W}_{kp}^{-1}$ **27**

4.1 Description of the KP Operator 27

4.1.1 Defining $\mathbf{W}_{kp}$ as a Composition 33

4.2 $\mathbf{W}_{kp}^{-1}$ 35

4.3 Formula for $\mathbf{W}_{kp}$ 36

4.4 Formula for $\mathbf{W}_{kp}^{-1}$ 37

5 Approximations for $\mathbf{W}_{kp}$ and $\mathbf{W}_{kp}^{-1}$ **38**

5.1 Description of $\mathbf{W}_n$ . . . 38

5.1.1 $\mathbf{W}_n$ an Approximation of $\mathbf{W}_{kp}$ . . . 40

5.2 $\mathbf{W}_n^{-1}$ . . . 41

5.2.1 Convergence, $u_n \rightarrow u^*$ . . . 42

5.2.2 $\mathbf{W}_n^{-1}$ Formulation using Discrete Measure . . . 43

6 Computer Simulation using the KP Operator **45**

6.1 Simulation Data . . . 45

6.2 The Parameter Identification Process . . . 46

6.3 Estimation of w using the Forward Operator $\mathbf{W}_n$. . . . 48

6.4 Estimation of u^* using the Inverse Operator $\mathbf{W}_n^{-1}$ . . . 48

7 Experimental Results for the KP Operator **52**

7.1 Experimental Data . . . 52

7.2 Parameter Identification . . . 54

7.3 Estimation of w using the Forward Operator $\mathbf{W}_n$ . . . 55

7.4 Estimation of u^* using the Inverse Operator $\mathbf{W}_n^{-1}$ . . . 56

8 Concluding Remarks **60**

9 Vita **62**

List of Figures

2.1 Actuator system 4
2.2 Input to actuator 5
2.3 Output of actuator with scalar hysteresis 5
2.4 I/O Hysteresis for an actuator 6
2.5 Find u^* such that $e = 0$ 6
2.6 Open loop control of an actuator with hysteresis 8

3.1 Input partition interval $[t_{k-1}, t_k]$ 10
3.2 Elementary hysteresis operator $\hat{\kappa}_\rho(u, \hat{\xi}_{k-1}(\rho))$, relay form 11
3.3 The Preisach plane 11
3.4 Step function $\hat{f}_2(u, \rho)$ u increasing. 13
3.5 Step function $\hat{f}_1(u, \rho)$ u decreasing. 13
3.6 $\hat{\xi}_0$, initial function 15
3.7 $\hat{\xi}_1$, function at $t = t_1$ 15
3.8 $\hat{\xi}_2$, function at $t = t_2$ 15
3.9 $\hat{\xi}_3$ at $t = t_3$ 16
3.10 Sequences of dominant maxima and minima 17
3.11 The Preisach plane partitioned by $L(t)$. 17
3.12 Vertical Strips E_V and Horizontal Strips E_H in the Preisach Plane 18
3.13 I/O curve for $w = \mathbf{P}(u; \hat{\xi}_{k-1})$ with $u \in I_{u_k}$ increasing, and $w \in I_{w_k}$ 19
3.14 Hysteresis loop produced by simulation 24

3.15 Input $w_d(t)$ (solid line) and output $w(t)$ (dashed line) for a system without compensation . . . 25
3.16 Compensating input, u^* . . . 26
3.17 Input $w_d(t)$ and output $w(t)$ for a system with compensation . . . 26

4.1 KP elementary operator . . . 28
4.2 Ridge function, r(u,x) . . . 29
4.3 ξ_0 . . . 29
4.4 Regions of $\mathcal{P}$ for an increasing input, $\Delta = \Delta_1 \cup \Delta_2 \cup \Delta_3$ . . . 31
4.5 Ridge function $f_2^{kp}(u, \rho)$ u increasing . . . 31
4.6 Ridge function $f_1^{kp}(u, \rho)$ u decreasing . . . 32
4.7 ξ_2 . . . 33
4.8 Level curve for $w = \mathbf{W}_{kp}(u; \xi_{k-1})$ with $u \in I_{u_k} = [u_{k-1}, u_k]$ increasing and $w \in I_{w_k}$ . . . 34

5.1 Open loop control of an actuator with hysteresis . . . 42
5.2 Open loop control using inverse approximation . . . 42

6.1 Bivariate sine input, u . . . 47
6.2 Bivariate input and output (u, w) . . . 47
6.3 Simulation input u . . . 49
6.4 Output w_n, reference input w_d and error $w_d - w_n$ generated with $\hat{\alpha}_i$ and α_i 49
6.5 Open loop control of an actuator with hysteresis . . . 50
6.6 Outputs $\hat{w}$ and w generated with $\hat{\alpha}_i$ and inverse $\hat{u^*}$ . . . 50
6.7 Input u_n generated by $u_n = \mathbf{W}_n^{-1}(w_d)$ . . . 51

7.1 Experimental Setup . . . 53
7.2 D800, D600, D400 I/O . . . 54
7.3 $\hat{w}$ estimate, w data and error for D800 data . . . 55
7.4 $\hat{w}$ estimate, w data and error for D600 data . . . 56
7.5 $\hat{w}$ estimate, w data and error for D400 data . . . 57

7.6 u , u_n and error for D800 data 58
7.7 u, u_n and error for D600 data 58
7.8 u, u_n and error for D400 data 59

8.1 Hybrid System for Parameter Identification 61

List of Tables

6.1 α_i for bivariate distribution $\bar{\rho}_1 = 0$ and $\bar{\rho}_2 = 0$, $\sigma = .6$ 46

6.2 Estimates for bivariate distribution, $\hat{\alpha}_i$ 48

7.1 Input Voltage Ranges for the Data Sets 53

7.2 Estimates $\hat{\alpha}_i$ using $D800$ data. 55

7.3 Data Sets and estimation errors for $max|w - \hat{w}|$ 56

7.4 Data Sets and estimation errors for compensated input u_n 57

Chapter 1

Overview

This dissertation investigates the use of inverse hysteresis operators as part of a strategy for controlling a system with hysteresis. Accurate control of a system that exhibits scalar hysteresis requires a control method that incorporates compensation for hysteresis. One approach is to develop a compensator based on an inverse hysteresis operator. This method uses an open loop control in which the inverse operation adjusts the actuator input to compensate for the hysteresis in the system. When this is accomplished, the composite operation produces an identity relationship between a reference input and the system output.

The use of inverse compensation to control a system with hysteresis is first demonstrated with the Preisach operator. In this case, an inverse for the Preisach operator is derived for a bivariate weighting function. Using a computer simulation, it is shown that the inverse provides the compensation necessary to reduce the effect of scalar hysteresis.

It is also shown that the inverse of a KP operator approximation can be used to provide compensation for hysteresis. Like the Preisach operator, an open loop control based on the inverse of the KP approximation is developed. It is verified by both a computer simulation, and experimental data obtained from a piezoelectric stack actuator, that this control provides the necessary compensation.

The principle contributions of this research are as follows;

- Development of an inverse Preisach operator for a bivariate weighting function.
- Demonstration that scalar hysteresis can be minimized by an open loop control method that is based on the inverse Preisach operator.
- Derivation of an inverse KP operator approximation using discrete measures.
- Demonstration that scalar hysteresis can be minimized by an open loop control method that is based on the inverse KP operator approximation. This was performed with both a computer simulation, and with experimental data from a piezoelectric stack actuator.

The essential aspects of this dissertation are organized in the following manner:

Chapter 2 provides an introduction to scalar hysteresis and defines the problem of controlling actuators with hysteresis. A solution to the control problem is then presented in the form of inverse compensation.

Chapter 3 provides an introduction to the Preisach operator. A Preisach operator is a versatile model capable of describing the macroscopic input/output (I/O) behavior of an actuator with scalar hysteresis. This chapter contains the description of the Preisach operator $\mathbf{P}$, proves that $\mathbf{P}^{-1}$ exists, develops a computational formula for $\mathbf{P}$ and $\mathbf{P}^{-1}$ using a bivariate weighting function, and uses a simulation to demonstrate inverse compensation.

Chapter 4 develops the KP operator $\mathbf{W}_{kp}$ and inverse $\mathbf{W}_{kp}^{-1}$. This operator (see Banks, Kurdila and Webb [1], [2]) allows the use of discrete measures for approximations and the computation of inverse operators.

In Chapter 5 the approximations $\mathbf{W}_n$ and $\mathbf{W}_n^{-1}$, for $\mathbf{W}_{kp}$ and $\mathbf{W}_{kp}^{-1}$ are developed using discrete measures, μ_n. The measures are approximated from experimental data based on the method developed by Banks, Kurdila and Webb [1], [2]. It is shown that the approximations are convergent and that the inverse provides a control input that compensates for hysteresis.

Chapter 6 demonstrates the capabilites of $\mathbf{W}_n$ and $\mathbf{W}_n^{-1}$ through the use of a computer simulation. The simulation demonstrates the ability of $\mathbf{W}_n$ to model hysteresis and the effectiveness of inverse compensation to minimize hysteresis.

Chapter 7 uses data collected from an actuator with scalar hysteresis to demonstrate the accuracy of the forward model $\mathbf{W}_n$, and to demonstrate the feasibility of using the inverse $\mathbf{W}_n^{-1}$ to provide the necessary compensation for reducing postitioning error created by hysteresis.

Chapter 8 presents concluding remarks directed at a method for adaptively estimating the parameters in the inverse $\mathbf{W}_n^{-1}$.

Chapter 2

Background

The problem of controlling a system that exhibits scalar hysteresis is presented and defined in terms of controlling devices called actuators.

The principle topics in this chapter are as follows:

- Description of scalar hysteresis;
- Defining the control problem for a 1-D actuator with scalar hysteresis;
- Proposing a solution to the control problem using inverse compensation.

2.1 Actuators and Scalar Hysteresis

In this work an actuator is a device that produces a physical displacement when a stimulus is applied. Common examples are motors and relays. Actuators are often used in positioning systems, and to actively control them it is necessary to have a model of the actuator. As a first step, the actuator will be treated as a "black box" entity, and the approach taken in modeling the actuator will focus on a global characterization of the actuator's I/O relationship.

A block representation of the acutator is shown in Figure 2.1. The input $u(t)$ is supplied to the actuator as a time varying voltage, current, or heat source. The actuator, represented as $\mathbf{W}$, reacts to an input by generating a displacement $w(t)$. In this work, actuators are restricted to the type that generate a continuous piecewise monotone displacement $w(t)$ (see Figure 2.3) when a continuous piecewise monotone input $u(t)$ (see Figure 2.2) is applied. For a single dimension of actuation, this relationship is given by the mapping

$$\mathbf{W} : C_{pm}[0,T]\mathtt{x}\xi_0 \rightarrow C_{pm}[0,T],$$

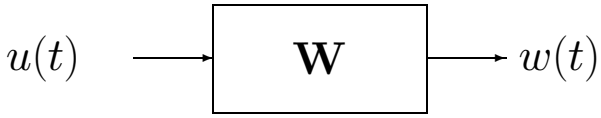

Figure 2.1: Actuator system

where the output $w(t)$ is given by $w(t) = [\mathbf{W}(u; \xi_0)](t)$ and ξ_0 is related to the initial state of the actuator. Here, $C_{pm}[0, T]$ denotes the space of continuous piecewise monotone functions on the interval $[0, T]$, with the norm $\|u\| = max_{t\in[0,T]}|u(t)|$.

Scalar Hysteresis a Physical Phenomena

If the graph of I/O data (u, w) is of the type shown in Figure 2.4, the actuator is considered to have the property of scalar I/O hysteresis. The principle characteristic of this graph is that as u increases ($\dot{u} > 0$) and decreases ($\dot{u} < 0$), a family of continuous connected curves are generated. Thus it appears that there is not a single function that models the relationship between w and u. Instead a family of functions are needed to represent the I/O relationship. More precisely, an actuator is considered to have the property of scalar hysteresis if it exhibits the following properties for a single dimension of actuation:

1. The inputs and outputs are continuous piecewise monotone functions $u, w \in C_{pm}[O, T]$.
2. The graphs of (u, w) lie within an envelope of admissible I/O curves that are bounded on the right by the curve Γ_r and on the left by the curve Γ_l as shown in Figure 2.4.
3. The shape of the I/O graph is independent of the rate of the input.
4. On intervals where u is strictly increasing or strictly decreasing, then so is the output w.

2.2 The Positioning Problem

For a simple positioning system consisting of a single actuator, it will be required that the actuator track a position reference signal $w_d(t)$ over an interval $[0, T]$. To accurately track $w_d(t)$, it is necessary to determine an input $u^*(t)$ for the actuator, such that the error between the actuator output and the reference, $e(t) = w_d(t) - w(t)$, is minimized. A block diagram for this system is shown in Figure 2.5.

The control problem addressed by this research is defined as follows:

Given an actuator, $\mathbf{W}$, with scalar hysteresis, find an input $u^*(t) \in C_{pm}[0, T]$ such that $\|[\mathbf{W}(u^*)](t) - w_d(t)\| \leq \|[\mathbf{W}(u)](t) - w_d(t)\|$ for $u(t) \in C_{PM}[0, T]$.

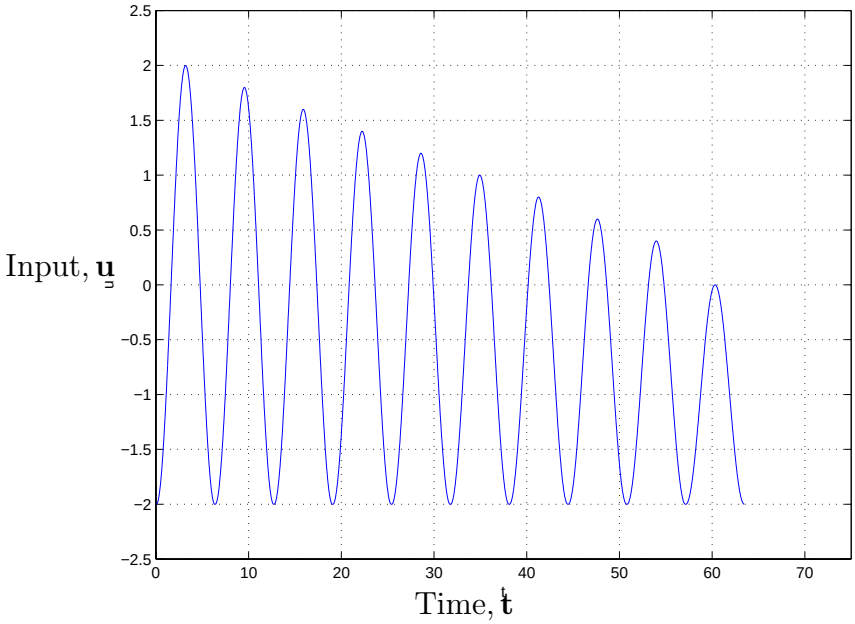

Figure 2.2: Input to actuator

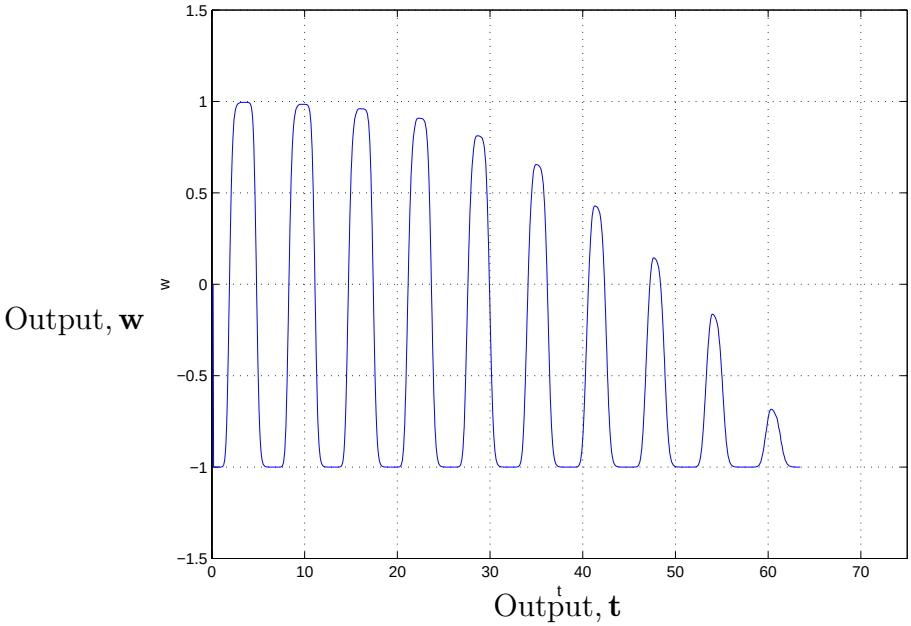

Figure 2.3: Output of actuator with scalar hysteresis

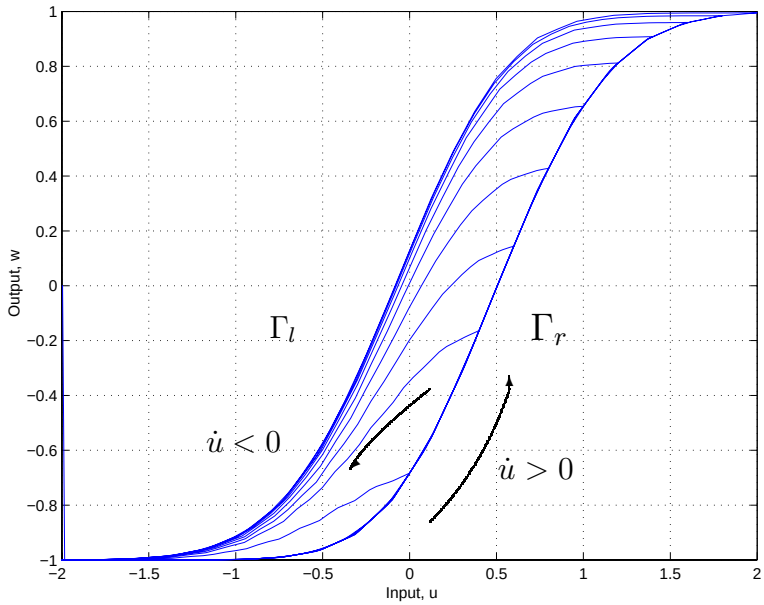

Figure 2.4: I/O Hysteresis for an actuator

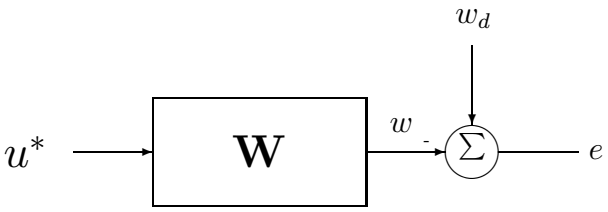

Figure 2.5: Find u^* such that $e = 0$

Next, it is proposed that $u^*(t)$ can be obtained by using the inverse of the hysteresis operator.

2.3 The Solution, Inverse Compensation

In recent years, several methods have emerged for controlling hysteretic actuators. These methods include, feedback controls based on Preisach models for SMA wire (Gorbet, Wang and Morris [3]); optimal controls based on physics models for magnetorestrictive actuators (Smith [4], [5]); adaptive closed loop controls using Preisach models for SMA wire (Lagoudas, Bo, Kurdila, Webb [6]); and open loop methods that use inverse compensation (Schäfer and Janocha [7]; Hughes and Wen [8]; Tao and Kokotović [9]; Galinaitis and Rogers [10], [11]). In the last approach, u^* is given by

$$u^*(t) = [\mathbf{W}^{-1}(w_d)](t)$$

where $\mathbf{W}^{-1}$ is the inverse operator of $\mathbf{W}$. Of course, u^* minimizes the error between the reference $w_d(t)$, and the actuator output, $w(t)$,

$$\begin{aligned} \|w(t) - w_d(t)\| &= \|[\mathbf{W}(u^*)](t) - w_d(t)\| && (2.1)\\ &= \|[\mathbf{W}(\mathbf{W}^{-1}(w_d)](t) - w_d(t)\| && (2.2)\\ &= \|w_d(t) - w_d(t)\| && (2.3)\\ &= 0 && (2.4) \end{aligned}$$

Thus,

$$\|[\mathbf{W}(u^*)](t) - w_d(t)\| = min_{u \in C_{pm}[0,T]} \|[\mathbf{W}(u)](t) - w_d(t)\|.$$

and so u^* is a minimizer. Therefore, it is a solution to the control problem.

If u^* can be found by using the inverse, the proposed control method for the actuator is an open loop control, as shown in Figure 2.6. The control consists of using w_d as input into the inverse $\mathbf{W}^{-1}(*)$ which in turn generates the actuator input u^*. As shown above, this produces an output w that is equal to the reference position w_d. If the actuator is accurately portrayed by the operator $\mathbf{W}$ and the inverse operator $\mathbf{W}^{-1}$ exists, then the composite operation produces a system that acts as an identity map and $w(t) = w_d(t)$.

To determine u^* in a real control situation, it is necessary to:

1. Find an operator $\mathbf{W}$ that accurately models the observed I/O curves and properties of an actuator;
2. Determine $\mathbf{W}^{-1}(*)$;
3. Develop approximations to the forward model, $\mathbf{W}_n$, and the inverse, $\mathbf{W}_n^{-1}$, for computer implementation;

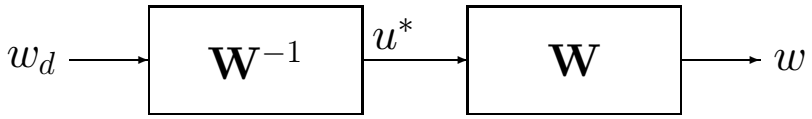

Figure 2.6: Open loop control of an actuator with hysteresis

4. Show that $w_n \to w$ for $w_n = \mathbf{W}_n(u)$ and $w = \mathbf{W}(u)$;
5. Prove that $u_n \to u^*$ for $u_n = \mathbf{W}_n^{-1}(w_d)$ and $u^* = \mathbf{W}^{-1}(w_d)$.

In the following chapters, two types of hysteresis operators (the Preisach and the KP) that fulfill the above requirements are developed. The ability of these operators to model scalar hysteresis, and generate the required input, u^*, is demonstrated through computer simulation and with experimental data from a piezoelectric actuator.

Chapter 3

Preisach Operator P and the Inverse $\mathbf{P}^{-1}$

The Preisach operator is a versatile model capable of describing the macroscopic I/O behavior of an actuator with scalar hysteresis. It has been used to model a variety of magnetic materials (Kádár [12], Della Torre [13], Della Torre and Vajda [14], [15], Della Torre,Vajda,Pardavi-Horvath and Lodder [16]) and solid-state energy transducers (Adly, Mayergoyz and Bergqvist [17], and Smith [4]). Their general properties have been discussed in a number of monographs including Mayergoyz [18]; Kransnosel'skiı and Pokrovskiı [19]; Visintin [20]; Brokate and Sprekels [21]; and Bertotti [22].

This chapter focuses on the following items:

- Description of the Preisach operator $\mathbf{P}$ and proof that $\mathbf{P}^{-1}$ exists;
- Development of a computational formula for $\mathbf{P}$;
- Development of $\mathbf{P}$ and $\mathbf{P}^{-1}$ using a bivariate weighting function;
- Demonstration of inverse compensation using computer simulation.

3.1 Description of the Preisach Operator P

The hysteresis operators of interest in this study map continuous piecewise monotone inputs to continuous piecewise monotone outputs on the interval $[0, T]$. Based on the characteristics of the input it is possible to define a partition of the interval $[0, T]$.

Let $\mathcal{T}$ be the partition of $[0, T]$ that is generated by requiring the subintervals $[t_{k-1}, t_k]$ to be the largest such that $u(t)$ is strictly monotone increasing, decreasing or constant, on any

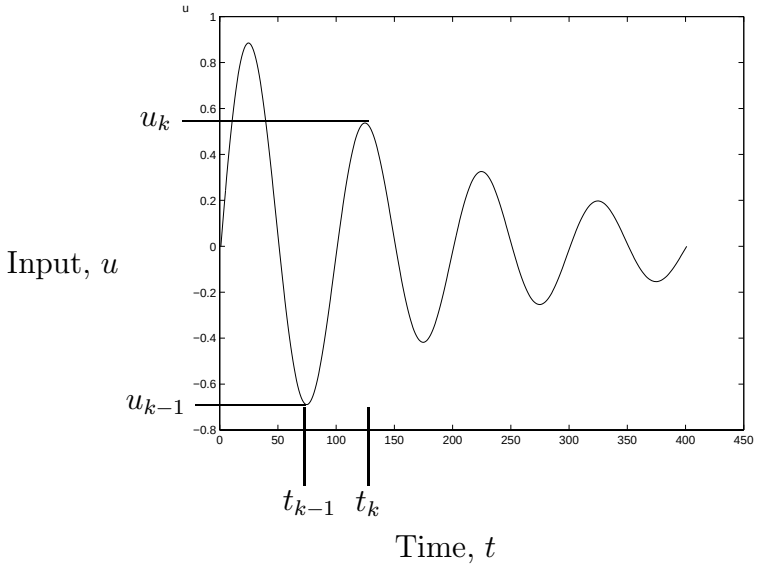

Figure 3.1: Input partition interval $[t_{k-1}, t_k]$

given subinterval as shown in Figure 3.1. The boundaries of the subintervals define a string S_T as follows.

$$S_T = \{t_0 = 0, t_1, \ldots, t_{k-1}, t_k, \ldots, t_N = T\}$$

For each value in S_T there is an input value $u_k = u(t_k)$ and output $w_k = w(t_k)$. The corresponding input string S_u is,

$$\hat{S}_u = \{u_0 = u(0), u_1, \ldots, u_{k-1}, u_k, \ldots, u_N = u(t_N)\}$$

and the output string is,

$$\hat{S}_w = \{w_0 = w(0), w_1, \ldots, w_{k-1}, w_k, \ldots, w_N = w(t_N)\}.$$

For each time interval $[t_{k-1}, t_k]$, the time interval is defined as $I_{t_k} = [t_{k-1}, t_k]$ and the corresponding input interval I_{u_k} is defined as,

$$I_{u_k} = [u_{k-1}, u_k]$$

and the output interval is given by,

$$I_{w_k} = [w_{k-1}, w_k].$$

If u is increasing on $[t_{k-1}, t_k]$, then $max(I_{u_k}) = u_k$ and $min(I_{u_k}) = u_{k-1}$. Similarly, if u is decreasing on an interval $[t_{k-1}, t_k]$, then $min(I_{u_k}) = u_k$ and $max(I_{u_k}) = u_{k-1}$. For the case where $u_k = u_{k-1}$ (u constant) I_{u_k} and I_{w_k} are sets containing single elements u_k and w_k. The Preisach operator, $\mathbf{P}$, is now defined for each interval I_{u_k}, in terms of a mapping from I_{u_k} to I_{w_k}.

Preisach Operator, **P**

The Preisach operator represents scalar hysteresis as the cummulative effect of weighted elementary hysteresis operators $\hat{\kappa}_\rho(u, \hat{\xi}_{k-1}(\rho))$ called relays (Krasnoselski and Pokrovski [19]).

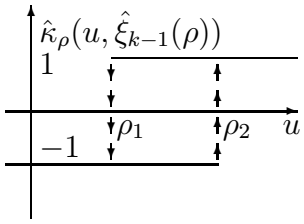

Figure 3.2: Elementary hysteresis operator $\hat{\kappa}_\rho(u, \hat{\xi}_{k-1}(\rho))$, relay form

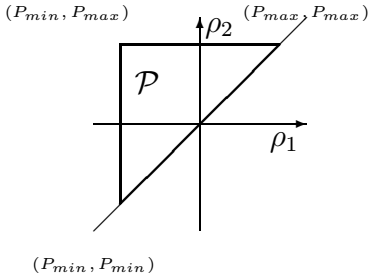

Figure 3.3: The Preisach plane

For $u \in I_{u_k}$, the operators $\hat{\kappa}_\rho(u, \hat{\xi}_{k-1}(\rho))$ map points $\rho = (\rho_1, \rho_2) \in R^2$ to the set $\{-1, 1\}$. The operator is defined as,

$$\hat{\kappa}_\rho(u, \hat{\xi}_{k-1}(\rho)) = \begin{cases} +1 & \rho_2 < u \\ \hat{\xi}_{k-1}(\rho) & \rho_1 \leq u \leq \rho_2 \\ -1 & u < \rho_1 \end{cases}$$

where $\hat{\xi}_{k-1}(\rho)$ is the state of a kernel at location $\rho = (\rho_1, \rho_2)$ for input u_{k-1}. The initial state, $\hat{\xi}_{k-1}(\rho)$, of a relay on the interval I_{u_k}, has a value of either a +1 or -1.

As shown in Figure 3.2, the graph of $\hat{\kappa}_\rho(u, \hat{\xi}_{k-1}(\rho))$ has two branches (+1 and -1) on which it remains constant as u increases or decreases, until it undergoes "irreversible" jumps at the parameter values ρ_1 and ρ_2. The parameters ρ_1 and ρ_2 are ordered with $\rho_2 \geq \rho_1$ and the set of feasible parameter pairs is,

$$\mathcal{P} = \{(\rho_1, \rho_2) \in R^2 \mid P_{min} \leq \rho_1 \leq \rho_2 \leq P_{max}\}$$

This set is called the *Restricted Preisach Plane* (see Figure 3.3). Since the input and output of the actuator are bounded, the values of (ρ_1, ρ_2) are also bounded. The lower bound, P_{min}, is equal to the minimum input value, and the upper bound P_{max} is equal to the maximum input value. For this discussion the term "restricted" will be dropped and this region will be referred to as the *Preisach plane*.

$\hat{\xi}_u$, a function defined on $\mathcal{P}$

If the input is brought to its minimum value, the kernels defined on $\mathcal{P}$ will take on the value of -1. Starting with this initial condition, the kernel values define a function $\hat{\xi}_0$ equal to -1 for all points in $\mathcal{P}$, $\hat{\xi}_0 \equiv 1$. For the interval $I_{u_1} = [u_0, u_1]$, a function $\hat{\xi}_u : \mathcal{P} \to \{-1, 1\}$ on $\mathcal{P}$ is calculated for a $u \in I_{u_1}$ by the following,

$$\hat{\xi}_u = \hat{\Phi}(u; \hat{\xi}_0)$$

where $\hat{\Phi}$ maps the current input, u and initial function, $\hat{\xi}_0$, to a new function $\hat{\xi}_u$ on $\mathcal{P}$

$$\hat{\Phi} : I_{u_1} \times \hat{S} \to \hat{S}.$$

The set $\hat{S}$ contains all possible measurable functions, $\hat{\xi}_u : \mathcal{P} \to \{-1, 1\}$, generated by the inputs $u(t) \in C_{pm}([0, T])$ and the mapping $\hat{\Phi}$. The exact form of $\hat{\Phi}$ depends on whether the input u is increasing or decreasing on an interval I_{u_k}. For an increasing input u, on the interval $[t_0, t_1]$

$$\hat{\Phi}(u; \hat{\xi}_0) := max_{\rho \in \mathcal{P}}\{\hat{f}_2(u, \rho), \hat{\xi}_0(\rho)\}$$

and for a decreasing input u on the interval $[t_0, t_1]$,

$$\hat{\Phi}(u; \hat{\xi}_0) := min_{\rho \in \mathcal{P}}\{\hat{f}_1(u, \rho), \hat{\xi}_0(\rho)\}.$$

The real valued functions $\hat{f}_2$ and $\hat{f}_1$ are step functions on $\mathcal{P}$. These functions are derived from $\hat{\kappa}_\rho(u, \hat{\xi}_{k-1}(\rho))$ and are defined next.

For an increasing input, the kernels define a discontinuous function $\hat{f}_2$ on $\mathcal{P}$. For $\rho_1 \in [P_{min}, P_{max}]$ the function $\hat{f}_2(u, (\rho_1, \rho_2))$ is a step function, $\hat{f}_2 : I_{u_k} \times \mathcal{P} \to \{-1, 1\}$ with,

$$\hat{f}_2(u, (\rho_1, \rho_2)) = \begin{cases} +1 & \rho_2 \leq u \\ -1 & u < \rho_2 \end{cases}$$

where $\rho_2 \in [\rho_1, P_{max}]$. An example of the function for a fixed ρ_1 is shown in Figure 3.4 (a). The function on the Preisach plane is formed by letting ρ_1 vary from P_{min} to P_{max}. It has the values of $+1$ for $\rho_2 \leq u$ and -1 for $u < \rho_1$. This function is shown in Figure 3.4(b).

The function $\hat{f}_1(u, \rho)$ is defined in a manner similar to $\hat{f}_2$. For each value $\rho_2 \in [P_{min}, P_{max}]$ we define the function $\hat{f}_1(u, (\rho_1, \rho_2))$ as,

$$\hat{f}_1 : I_{u_k} \times \mathcal{P} \to \{-1, 1\}$$

$$\hat{f}_1(u, (\rho_1, \rho_2)) = \begin{cases} +1 & \rho_1 \leq u \\ -1 & u < \rho_1 \end{cases}$$

with $\rho_1 \in [P_{min}, \rho_2]$. Like $\hat{f}_2$, the function $\hat{f}_1$ is a discontinuous function on $\mathcal{P}$. An example of the function is shown in Figure 3.5 (a) for a fixed value of ρ_2. It has the values of $+1$ for $\rho_1 \leq u$ and -1 for $u < \rho_1$. The function on the Preisach plane is formed by letting ρ_2

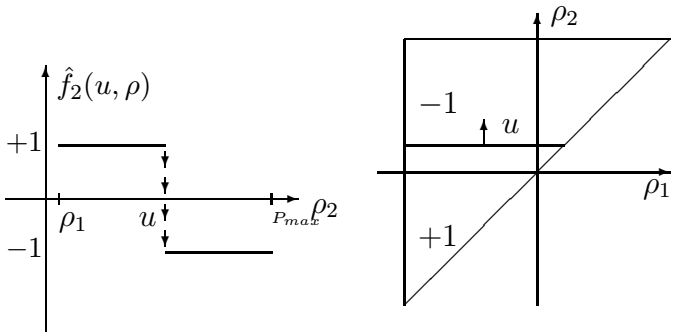

(a) $\hat{f}_2(u,\rho)$ (b) Function $\hat{f}_2(u,\rho)$

Figure 3.4: Step function $\hat{f}_2(u,\rho)$ u increasing.

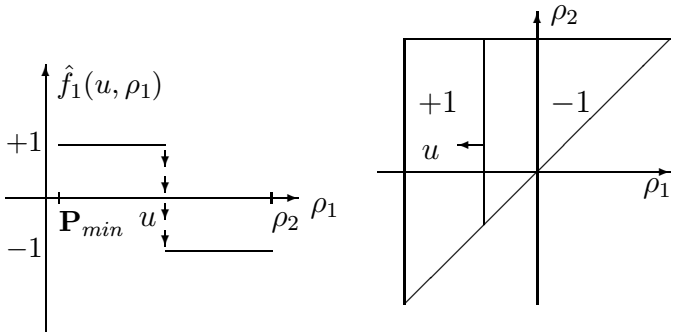

(a) $\hat{f}_1(u,\rho)$ (b) Function generated by $\hat{f}_1(u,\rho)$

Figure 3.5: Step function $\hat{f}_1(u,\rho)$ u decreasing.

vary from P_{min} to P_{max}. This function is shown in Figure 3.5(b). For $u \in I_{u_k}$, the function $\hat{\xi}_u$ is simply generated by comparing $\hat{f}_1$ or $\hat{f}_2$ to the initial set of kernel values $\hat{\xi}_0$. For any interval I_{u_k}, the function $\hat{\xi}_u : \mathcal{P} \to \{-1, 1\}$ is generated by,

$$\hat{\xi}_u = \hat{\Phi}(u; \hat{\xi}_{k-1})$$

where the initial function $\hat{\xi}_{k-1}$ is

$$\hat{\xi}_{k-1} = \hat{\Phi}(u_{k-1}; \hat{\xi}_{k-2}).$$

For an increasing input u, on the interval $[t_{k-1}, t_k]$,

$$\hat{\Phi}(u; \hat{\xi}_{k-1}) := max_{\rho \in \mathcal{P}}\{\hat{f}_2(u, \rho); \hat{\xi}_{k-1}(\rho)\}$$

and for a decreasing input $u(t)$,

$$\hat{\Phi}(u; \hat{\xi}_k) := min_{\rho \in \mathcal{P}}\{\hat{f}_1(u, \rho); \hat{\xi}_{k-1}(\rho)\}.$$

As the input u varies over each subinterval I_{u_k} the resulting function $\hat{\xi}_u$ is a composite of the preceding sequence of functions. Not all of the previous functions are necessary for determining the current function $\hat{\xi}_u$. A property of the Preisach operator is that the final function is dependent only on a subset of the input local maxima and minima, and through their related functions.

Memory and the Wiping Out Property

An important property of the Preisach model is that the function $\hat{\xi}_u$ on $\mathcal{P}$ is dependent only on the current input, and past sequences of decreasing input local maximas and increasing input local minima.

Let the input $u(t)$ be as shown in Figure 3.6(a). Initially, the input $u(0) = P_{min}$, and the system of relays is in a negative saturation state, giving an initial function $\hat{\xi}_0$, where $\hat{\xi}_0(\rho) \equiv -1$, for all $\rho \in \mathcal{P}$ as shown in Figure 3.6(b).

If the input $u(t)$ increases over the interval $[t_0, t_1]$ the mapping $\hat{\Phi}(u; \hat{\xi}_0)$ generates the function $\hat{\xi}_u$ shown in Figure 3.7(b). The function achieved at the maximum u_1 is $\hat{\xi}_1 = \hat{\Phi}(u_1; \hat{\xi}_0)$. As $u(t)$ decreases on the interval $[t_1, t_2]$ it reaches a local minima at t_2. This function is given as $\hat{\xi}_2 = \hat{\Phi}(u_2; \hat{\xi}_1)$ and is shown in Figure 3.8(b).

The coordinates $(P_{min}, M_1), (m_1, M_1), (m_1, m_1)$ define a line $L(t)$ in $\mathcal{P}$. $L(t)$ partitions $\mathcal{P}$ into regions $\mathcal{P}^+$, and $\mathcal{P}^-$, where $\hat{\xi}_u(\rho) = +1$ in $\mathcal{P}^+$ and $\hat{\xi}_u(\rho) = -1$ in $\mathcal{P}^-$. As u increases on $[t_2, t_3]$ u exceeds M_1 (see Figure 3.9(a)). At this point the effect of the previous inputs in forming the function $\hat{\xi}_u$ are all removed and $\hat{\xi}_u$ is dependent only on u and $\hat{\xi}_0$ (see Figure 3.9(b)). This effect is known as the wiping out property. In general, the function $\hat{\xi}_u$ depends on a sequence of dominant local input maxima, and a sequence of dominant local input minima (see Figure 3.10). For $u(t) \in C_{PM}[0, T]$ it can be shown that):

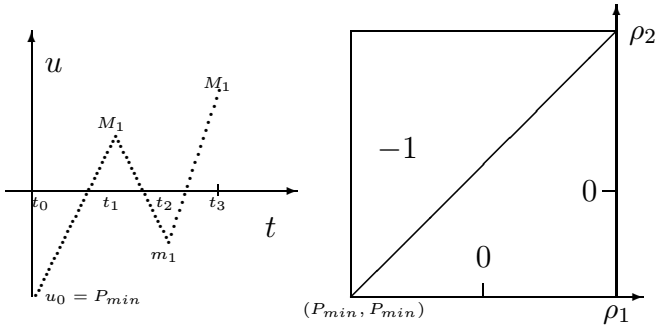

(a) $u(t)$ (b) $\hat{\xi}_0(\rho) = -1$

Figure 3.6: $\hat{\xi}_0$, initial function

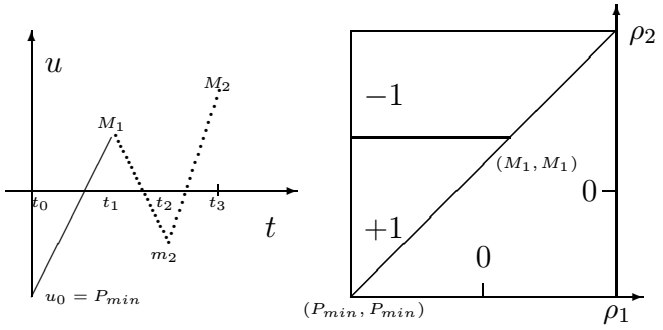

(a) $u(t)$ for $t \in [t_0, t_1]$ (b) $\hat{\xi}_1$, u_1

Figure 3.7: $\hat{\xi}_1$, function at $t = t_1$

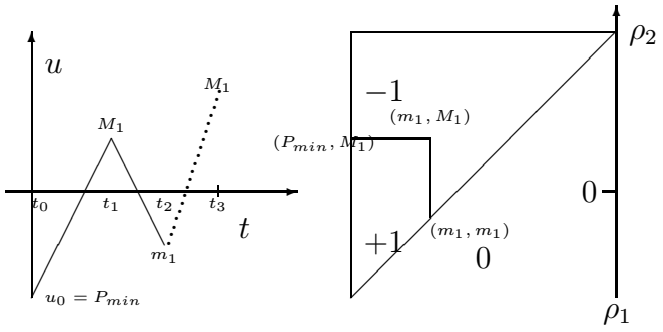

(a) $u(t)$ (b) $\hat{\xi}_2$, u_2

Figure 3.8: $\hat{\xi}_2$, function at $t = t_2$

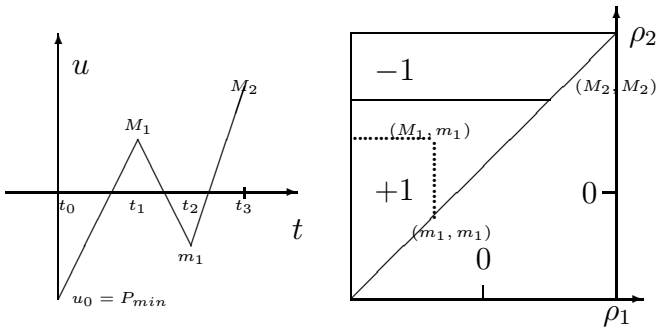

(a) $u(t)$ (b) $\hat{\xi}_3(\rho)$

Figure 3.9: $\hat{\xi}_3$ at $t = t_3$

- If $\dot{u}(t) > 0$, there is a sequence of times

$$0 < t^1 < t_1 < t^2 < t_2 < \cdots < t^{k-1} < t_{k_t-1} < t^{k_t} = t$$

such that

$$u(t^i) > u(t^{i+1}), \quad i = 1, \ldots, k_t - 1,$$
$$u(t_i) < u(t_{i+1}), \quad i = 1, \ldots, k_t - 2,$$

and

$$u(t_i) \leq u(t) \leq u(t^{i+1}), \text{ for } t \in [t_i, t^{i+1}], \ \ i = 1, \ldots, k_{t-1},$$
$$u(t_i) \leq u(t) \leq u(t^i), \text{ for } t \in [t^i, t_i], \ \ i = 1, \ldots, k_{t-1}.$$

- If $\dot{u}(t) < 0$, there is a sequence of times

$$0 < t^1 < t_1 < t^2 < t_2 < \cdots < t^{k_t-1} < t_{k_t-1} < t^{k_t} < t_{k_t} = t$$

such that

$$u(t^i) > u(t^{i+1}), \quad i = 1, \ldots, k_{t-1},$$
$$u(t_i) < u(t_{i+1}), \quad i = 1, \ldots, k_{t-1},$$

and

$$u(t_i) \leq u(t) \leq u(t^{i+1}), \text{ for } t \in [t_i, t^{i+1}], \ \ i = 1, \ldots, k_{t-1},$$
$$u(t_i) \leq u(t) \leq u(t^i), \text{ for } t \in [t^i, t_i], \ \ i = 1, \ldots, k_t.$$

Define

$$M_i = u(t^i), \quad i = 1, 2, \ldots, k_t,$$

as the local maximas and

$$m_i = u(t_i), \quad i = 1, 2, \ldots, k_{t-1},$$

as the local minimas. The sequences are denoted by $\mathcal{M}_{\max} := \{M_i\}_{i=1}^{k_t}$ and $\mathcal{M}_{\min} := \{m_i\}_{i=1}^{k_t-1}$. These sequences are a decreasing sequence of dominant local maxima and an

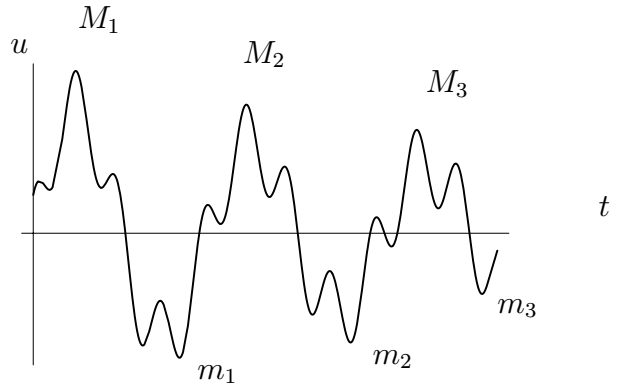

Figure 3.10: Sequences of dominant maxima and minima

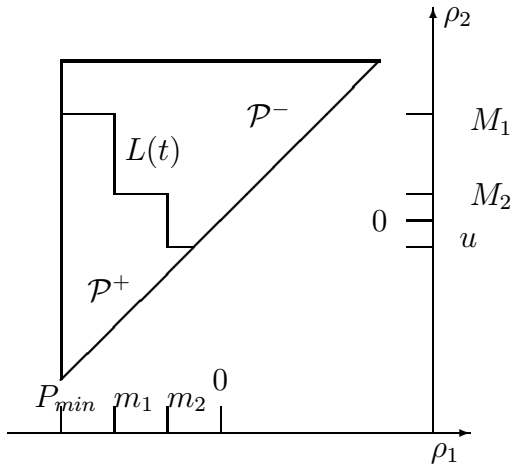

Figure 3.11: The Preisach plane partitioned by $L(t)$.

increasing sequence of dominant local minima respectively, (see Figure 3.10). The sequences change as a function of $u(t)$. As seen in the preceding example, whenever $u(t)$ exceeds an element $M_i \in \mathcal{M}$, all the elements M_j for $j \geq i$ are removed from $\mathcal{M}_{\max}$ and all the elements m_j for $j \geq i$ are removed from $\mathcal{M}_{\min}$. Similarly, whenever $u(t)$ falls below an element $m_i \in \mathcal{M}_{\min}$, all the elements M_j for $j > i$ are removed from $\mathcal{M}_{\max}$ and all the elements m_j for $j \geq i$ are removed from $\mathcal{M}_{\min}$. Thus, the number of elements in the sequences k_t changes with time. This property of the Preisach model is known as the wiping out property. The sets $\mathcal{M}_{\min}$ and $\mathcal{M}_{\max}$ define a polygonal curve $L(t)$ with vertices located at the extremal coordinates, $(P_{\min}, M_1)$, (m_1, M_1), (m_1, M_2), $(m_2, M_2), \ldots,$ (m_{k_t-1}, M_{k_t-1}), (m_{k_t-1}, M_{k_t}), (M_{k_t}, M_{k_t}) if $\dot{u}(t) > 0$ and $(P_{\min}, M_1)$, (m_1, M_1), (m_1, M_2), $(m_2, M_2), \ldots,$ (m_{k_t-1}, M_{k_t-1}), and (m_{k_t}, m_{k_t}) if $\dot{u}(t) < 0$. This curve partitions the Preisach plane into the two regions, $\mathcal{P}^+$ where all of the relays are in the $+1$ state, and $\mathcal{P}^-$ where all of the relays are in the -1 state (see Figure 3.11).

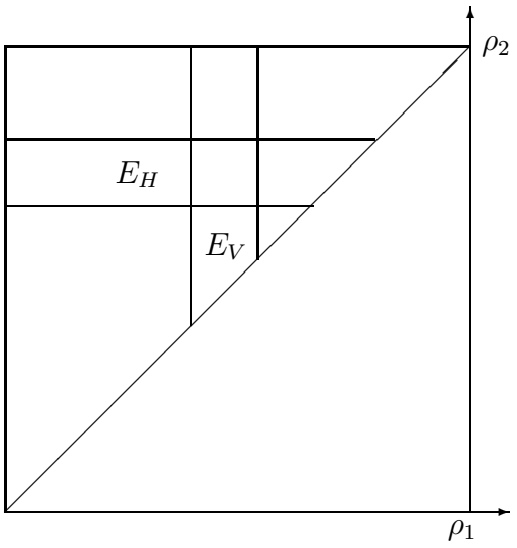

Figure 3.12: Vertical Strips E_V and Horizontal Strips E_H in the Preisach Plane

3.1.1 The Preisach Operator Defined as a Composition.

The Preisach operator for each $u \in I_{u_k}$ is now defined as the composition of an operator $\hat{\Phi}$ that maps functions on the Preisach plane, to the same, and the functional Λ_μ that maps those functions to $w \in I_{w_k}$. Define the functional Λ_μ as,

$$\Lambda_\mu(\hat{\xi}_u) := \int_{\mathcal{P}} \hat{\xi}_u(\rho) d\mu(\rho)$$

where Λ_μ maps the function $\hat{\xi}_u : \mathcal{P} \to \{-1, 1\}$ to $w \in I_{w_k}$,

$$\Lambda_\mu : \hat{S} \to I_{w_k}.$$

The measure μ is in $\mathcal{M}$ the set of probability measures associated with the probablity space $\{\mathcal{P}, \mathcal{B}(\mathcal{P}), \mu\}$. Due to the discontinuity of the function $\hat{\xi}_u$ and the requirement that $\mathbf{P}$ must be a continuous function from I_{u_k} to I_{w_k}, the measure μ must be zero for vertical and horizontal lines in $\mathcal{P}$ (Visintin [20]),

$$\mu(R \text{ x } \{r\}) = \mu(\{r\} \text{ x } R) = 0, \text{ for every } r \in R$$

Additionally, to maintain the strict monotonicity of the output for a strictly monotone input, the measure must be non-zero on horizontal strips, E_H, extending from a left vertical boundary given by the previous minima, m, to the diagonal, and vertical strips, E_V, extending from the diagonal to previous maxima, M, (see Figure 3.12).

The Preisach operator $\mathbf{P}$ is a composition given as, $\mathbf{P}(u; \hat{\xi}_{k-1}) = \Lambda_\mu \circ \hat{\Phi}(u; \hat{\xi}_{k-1})$ and $w =$

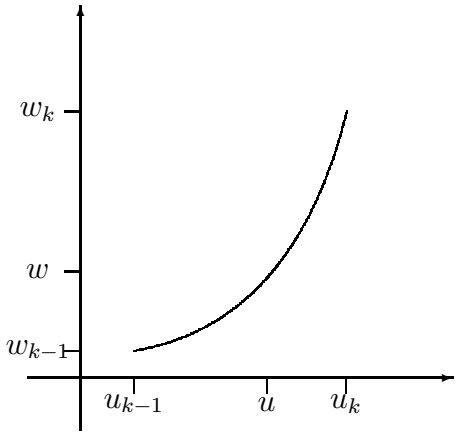

Figure 3.13: I/O curve for $w = \mathbf{P}(u; \hat{\xi}_{k-1})$ with $u \in I_{u_k}$ increasing, and $w \in I_{w_k}$

$\mathbf{P}(u; \hat{\xi}_{k-1})$.

$\mathbf{P}$ is a real valued function that maps $u \in I_{u_k}$ and $\hat{\xi}_u \in \hat{S}$ to $w \in I_{w_k}$, and by the above compositions the output w is calculated by integrating $\hat{\xi}_u$ over the Preisach plane,

$$w = \int_{\rho \in \mathcal{P}} \hat{\xi}_u(\rho) d\mu(\rho). \tag{3.1}$$

An I/O curve generated by Equation 3.1 for an increasing input is shown in Figure 3.13. A similar type of curve is produced for a decreasing input. It will be shown that there is only a single curve for each interval I_{u_k}, and this fact will allow an inverse to be calculated for $\mathbf{P}$ on intervals, I_{u_k}. On intervals where $\dot{u}(t) \neq 0$ the function $u(t)$ is a continuous bijective function from an interval $[t_{k-1}, t_k]$ to the interval $[u_{k-1}, u_k]$ and $w(t) = [\mathbf{P}(u; \hat{\xi}_{k-1})](t)$. On intervals where $\dot{u}(t) = 0$, $u(t) = u(t_{k-1})$ and $w(t) = [\mathbf{P}(u_{k-1}, \hat{\xi}_{k-1})](t)$ on this interval. Therefore, with respect to the interval $[t_{k-1}, t_k]$ the Preisach operator, $\mathbf{P}$, is the mapping

$$\mathbf{P}(*; \hat{\xi}_{k-1}) : C_{pm}[t_{k-1}, t_k] \rightarrow C_{pm}[t_{k-1}, t_k].$$

In the following discussions the time dependency is assumed and the Preisach operator will often be discussed with respect to the input interval I_{u_k}.

Not to lose sight of the goal, the objective is to find the inverse hysteresis operator so that inverse compensation can be used to generate the input u^* that minimizes the effect of hysteresis. First it is necessary to show that $\mathbf{P}$ has an inverse.

3.2 $\mathbf{P}^{-1}$

Because of the wiping out property, a Preisach operator can only be locally invertible. Fortunately, this type of invertibility is enough for the actuator positioning problem. The existence

of $\mathbf{P}^{-1}$ from I_{w_k} to I_{u_k} is shown by proving that $\mathbf{P}$ is a continuous bijective function from interval I_{u_k} to the interval I_{w_k}. So, first it is shown that $\mathbf{P}$ is **1-1** on each interval I_{u_k}.

Theorem 3.1 *For $\hat{\xi}_{k-1} \in \hat{S}$, $I_{u_k} \ni u \rightarrow \mathbf{P}(u; \hat{\xi}_{k-1}) \in I_{w_k}$ is $\mathbf{1-1}$.*

Proof:
Let $u_1, u_2 \in I_{u_k}$. Suppose $w_2 = w_1$ and $u_1 < u_2$.

Then

$$\begin{aligned} 0 &= \mid w_2 - w_1 \mid & (3.2)\\ &= \mid \mathbf{P}(u_2; \hat{\xi}_{k-1}) - \mathbf{P}(u_1; \hat{\xi}_{k-1}) \mid & (3.3)\\ &= \mid \int_{\mathcal{P}} \hat{\xi}_{u_2}(\rho) - \hat{\xi}_{u_1}(\rho) d\mu \mid & (3.4) \end{aligned}$$

If the two functions differ, it will be on a set $E \in \{E_H\}$ for $\dot{u} > 0$ or $E \in \{E_V\}$ for $\dot{u} < 0$. Continuing,

$$\begin{aligned} 0 &= \mid \int_{\mathcal{P}-E} \hat{\xi}_{u_2}(\rho) - \hat{\xi}_{u_1}(\rho) d\mu + \int_E \hat{\xi}_{u_2}(\rho) - \hat{\xi}_{u_1}(\rho) d\mu \mid & (3.5)\\ &= \mid \int_E \hat{\xi}_{u_2}(\rho) - \hat{\xi}_{u_1}(\rho) d\mu \mid & (3.6)\\ &= \int_E 2 d\mu & (3.7)\\ 0 &= 2\mu(E) & (3.8) \end{aligned}$$

The last equality is true only if $\mu(E) = 0$ for any $E \in \{E_H\}$ or $E \in \{E_V\}$ depending on whether u is increasing or decreasing. Since $\mu(E) > 0$, for these sets, the assumption that $u_2 > u_1$ must be false. Therefore, $u_1 = u_2$ and $\mathbf{P}$ is **1-1** on the interval I_{u_k}. ♣

Next it is shown that $\mathbf{P}$ is **continuous** on I_{u_k}.

Theorem 3.2 *For $\hat{\xi}_{k-1} \in \hat{S}, I_{u_k} \ni u \rightarrow \mathbf{P}(u : \hat{\xi}_{k-1}) \in I_{w_k}$ is continuous.*

Proof:
Let $\{u_n\}$ be a sequence in I_{u_k} such that $u_n \rightarrow u^*$ with $u^* \in I_{u_k}$. Let $\hat{\xi}_n \in \hat{S}$ be the sequence of functions on $\mathcal{P}$ generated by $\hat{\xi}_n = \hat{\Phi}(u_n; \hat{\xi}_{k-1})$ and $\hat{\xi}_{u^*} = \hat{\Phi}(u^*; \hat{\xi}_{k-1})$, $\hat{\xi}_{u^*} \in \hat{S}$.

By the definition of $\hat{\xi}_u$ it can be shown that

$$\lim_{n \rightarrow \infty} \hat{\xi}_n(\rho) = \hat{\xi}_{u^*}(\rho)$$

for every $\rho \in \mathcal{P}$. Next, let $g(\rho) = 1$ for all $\rho \in \mathcal{P}$. Then $\mid \hat{\xi}_n(\rho) \mid \leq g(\rho)$. Since the $\hat{\xi}_n$ and $\hat{\xi}_u$ are measurable functions on $\mathcal{P}$,

$$\lim_{n \rightarrow \infty} w_n = \lim_{n \rightarrow \infty} \int_{\mathcal{P}} \hat{\xi}_n d\mu = \int_{\mathcal{P}} \hat{\xi}_{u^*} d\mu = w^*$$

by the Lebesgue Convergence Theorem. Thus for any sequence $u_n \to u^*$ in I_{u_k} we have $w_n \to w^*$ in I_{w_k}. So $\mathbf{P}$ is sequentially continuous at u^* and therefore it is continuous at any u^* in I_{u_k}. ♣

Since $\mathbf{P}$ is continuous and **1-1** on the closed interval I_{u_k}, $\mathbf{P}$ is onto the interval I_{w_k}, and therefore $\mathbf{P}$ is a bijective function from I_{u_k} to I_{w_k}.

Theorem 3.3 $\mathbf{P}(*;\hat{\xi}_{k-1}) : I_{u_k} \to I_{w_k}$ *has a unique inverse* $\mathbf{P}^{-1}(*;\hat{\xi}_{k-1}) : I_{w_k} \to I_{u_k}$.

Proof:
$\mathbf{P}$ is bijective from I_{u_k} to I_{w_k}, therefore, it has a unique inverse,$\mathbf{P}^{-1} : I_{w_k} \to I_{u_k}$. ♣

3.3 The Computational Formula for the Forward Model

For any $\hat{\xi}_u : \mathcal{P} \to \{-1, 1\}$ we partition $\mathcal{P}$ into two regions, $\mathcal{P}^+$ and $\mathcal{P}^-$, where $\mathcal{P}^+ \cup \mathcal{P}^- = \mathcal{P}$ and

$$\hat{\xi}_u(\rho) = \begin{cases} 1 & \rho \in \mathcal{P}^+ \\ -1 & \rho \in \mathcal{P}^- \end{cases} \tag{3.9}$$

Then, for $u \in I_{u_k}$,

$$\begin{aligned} w &= \mathbf{P}(u;\hat{\xi}_{k-1}) && (3.10)\\ &= \int_{\mathcal{P}} \hat{\xi}(\rho) d\mu(\rho) && (3.11)\\ &= \int_{\mathcal{P}^+} d\mu(\rho) - \int_{\mathcal{P}^-} d\mu(\rho) && (3.12) \end{aligned}$$

then using the fact that,

$$1 - \int_{\mathcal{P}^+} d\mu(\rho) = \int_{\mathcal{P}^-} d\mu(\rho)$$

we obtain,

$$w = 2\int_{\mathcal{P}^+} d\mu(\rho) - 1.$$

To calculate the value of w it is necessary to either estimate μ or assume some function for μ. (See Mayergoyz [18], Hughes and Wen [8], and Della Torre,Oti and Kádár [23]).

For the space $(\mathcal{P}, B(\mathcal{P}), \mu)$, if the measure μ is absolutely continuous with respect to Lebesgue measure then there is a non-negative measurable function $\nu(\rho_2, \rho_1)$ such that for each set E in $B(\mathcal{P})$ we have $\mu(E) = \int_E \nu(\rho_1, \rho_2) d\rho_1 d\rho_2$. The Preisach operator can then be written as,

$$\mathbf{P}(u;\hat{\xi}_{k-1}) := \int\int_{(\rho_1,\rho_2)\in\mathcal{P}} \nu(\rho_1, \rho_2)\hat{\xi}_u(\rho_1, \rho_2)\, d\rho_1\, d\rho_2. \tag{3.13}$$

Here $\nu(\rho_1, \rho_2)$ is called the *weighting function* or Preisach function. As the name implies, the function ν gives a weight to the various relays at each point in $\mathcal{P}$. It is the distribution of these weights, that determines the global character of the hysteresis loops. Using the Preisach function $\nu(\rho_1, \rho_2)$ Equation 3.12 becomes

$$w = \int\int_{(\rho_1,\rho_2)\in\mathcal{P}^+} \nu(\rho_2, \rho_1)\, d\rho_2\, d\rho_1 - \int\int_{(\rho_1,\rho_2)\in\mathcal{P}^-} \nu(\rho_2, \rho_1)\, d\rho_2\, d\rho_1. \tag{3.14}$$

then since $\mu(\mathcal{P}) = 1$,

$$1 - \int\int_{(\rho_1,\rho_2)\in\mathcal{P}^+} \nu(\rho_1, \rho_2)\, d\rho_2\, d\rho_1 = \int\int_{(\rho_1,\rho_2)\in\mathcal{P}^-} \nu(\rho_1, \rho_2)\, d\rho_2\, d\rho_1$$

and it is possible to obtain by substitution,

$$w = 2\int\int_{(\rho_1,\rho_2)\in\mathcal{P}^+} \nu(\rho_1, \rho_2)\, d\rho_2\, d\rho_1 - 1.$$

This expression is further simplified, if for $a \geq b$ we define

$$w_{b,a} := 2\int_{P_{\min}}^{b}\int_{\rho_1}^{a} \nu(\rho_1, \rho_2)\, d\rho_2\, d\rho_1. \tag{3.15}$$

In this case, the output, w, can now be expressed as the sum of the $w_{b,a}$ evaluated at the local maxima and minima (see Mayergoyz [18], and Hughes and Wen [8])

$$w = \{\sum_{i=1}^{k_t-1} [w_{m_i,M_i} - w_{m_{i-1},M_i}] + \Delta w\} - 1 \tag{3.16}$$

where

$$\Delta w := \begin{cases} w_{u,u} - w_{m_{k_t-1},u} & \text{if } \dot{u} > 0, \\ w_{u,M_{k_t}} - w_{m_{k_t-1},M_{k_t}} & \text{if } \dot{u} < 0, \\ 0 & \text{if } \dot{u} = 0. \end{cases} \tag{3.17}$$

Because of the dependence of $\hat{\xi}_u$ on the past history of u, Equation (3.13) tends to be a difficult formula with which to compute. To simplify matters it is assumed that $u(0) = P_{\min}$ and that $\hat{\xi}_0(\rho) = -1$.

3.4 Forward and Inverse Models using the Bivariate Density Function.

A weighting function that is often used in the modeling of ferromagnetic devices is given by a bivariate distribution (see Della Torre and Vajda [24],and Oti and Kádár [23]).

The weighting function is,

$$\nu(\rho_1, \rho_2) := \begin{cases} \frac{1}{2\pi\sigma} \exp\left[-\frac{1}{2}\left(\frac{(\rho_2-\gamma)^2}{\sigma^2} + \frac{(\rho_1+\gamma)^2}{\sigma^2}\right)\right] & \rho_2 \geq 0,\ \ \rho_1 \leq 0, \\ 0 & \text{elsewhere} \end{cases} \tag{3.18}$$

where the center of the weighting function is at $(\gamma, -\gamma)$. Here $\sigma << \gamma$ such that $1 \approx \int\int_{(\rho_1,\rho_2)\in\mathcal{P}_{2nd}} \nu(\rho_1, \rho_2)\, d\rho_2\, d\rho_1$.

If $\dot{u} > 0$ we can calculate from (3.14) and (3.17)

$$\Delta w = \begin{cases} \frac{1}{2}\left[\operatorname{erf}\left(\frac{u-\gamma}{\sqrt{2}\sigma}\right) + \operatorname{erf}\left(\frac{\gamma}{\sqrt{2}\sigma}\right)\right]\left[\operatorname{erf}\left(\frac{\gamma}{\sqrt{2}\sigma}\right) - \operatorname{erf}\left(\frac{m_{k_t-1}+\gamma}{\sqrt{2}\sigma}\right)\right] & u > 0 \\ 0 & u \leq 0. \end{cases} \tag{3.19}$$

Similarly if $\dot{u} < 0$ the change in the output is,

$$\Delta w = \begin{cases} -\frac{1}{2}\left[\operatorname{erf}\left(\frac{M_{k_t}-\gamma}{\sqrt{2}\sigma}\right) + \operatorname{erf}\left(\frac{\gamma}{\sqrt{2}\sigma}\right)\right]\left[\operatorname{erf}\left(\frac{\gamma}{\sqrt{2}\sigma}\right) - \operatorname{erf}\left(\frac{u+\gamma}{\sqrt{2}\sigma}\right)\right] & u < 0 \\ 0 & u > 0. \end{cases} \tag{3.20}$$

The output w is then calculated using Equation 3.16. This model produces hysteresis loops of the type exhibited in Figure 3.14. Note that the weighting function is zero outside of the second quadrant of the Preisach plane, and this causes the loops to exhibit a pronounced saturation effect.

The two parameters γ and σ give independent control over two characteristics of the loop shape. The width of the loop is controlled by γ. The input required to drive the major loop to a zero output (the "coercive field" in ferromagnetism) is $\pm\gamma$ so that the width of the loop is 2γ. The "squareness" of the loop is controlled by σ. The parameter σ is identified by using the following equation developed by Oti[25],

$$\sigma = \frac{|u(\bar{t}) - \gamma|}{\sqrt{2\ln\left(\frac{c_0}{c}\right)}}. \tag{3.21}$$

Here c_0 is the slope of the ascending major loop at the coercive input γ and c is the slope of the ascending major loop at another input $u(\bar{t}) \neq \gamma$. For the case where $\dot{w} > 0$ and $u_{k-1} < 0$ the input is initially set to $u = 0$, since no inverse for $\mathbf{P}$, exists in the third quadrant. Similarly, when $\dot{w} < 0$ and $u_{k-1} > 0$ the input is initally set to $u = 0$, since no inverse exists in the first quadrant either.

3.4.1 Computation of the Inverse

For the bivariate weighting function it is possible to find a closed form formula for the inverse operator for the second quadrant. The closed form inverse is calculated for $\mathbf{P}$ by solving for u in the preceeding equations (3.19 and 3.20). The result is as follows,

$$u = \mathbf{P}^{-1}(w) := \begin{cases} \sqrt{2}\sigma \operatorname{ierf}\left(\frac{2\Delta w}{\mathcal{K}_1} - \operatorname{erf}\left(\frac{\gamma}{\sqrt{2}\sigma}\right)\right) + \gamma & \dot{w} \geq 0 \\ \sqrt{2}\sigma \operatorname{ierf}\left(\frac{2\Delta w}{\mathcal{K}_2} + \operatorname{erf}\left(\frac{\gamma}{\sqrt{2}\sigma}\right)\right) - \gamma & \dot{w} \leq 0 \end{cases} \tag{3.22}$$

where

$$\mathcal{K}_1 := \operatorname{erf}\left(\frac{\gamma}{\sqrt{2}\sigma}\right) - \operatorname{erf}\left(\frac{m_{k_t-1}+\gamma}{\sqrt{2}\sigma}\right)$$

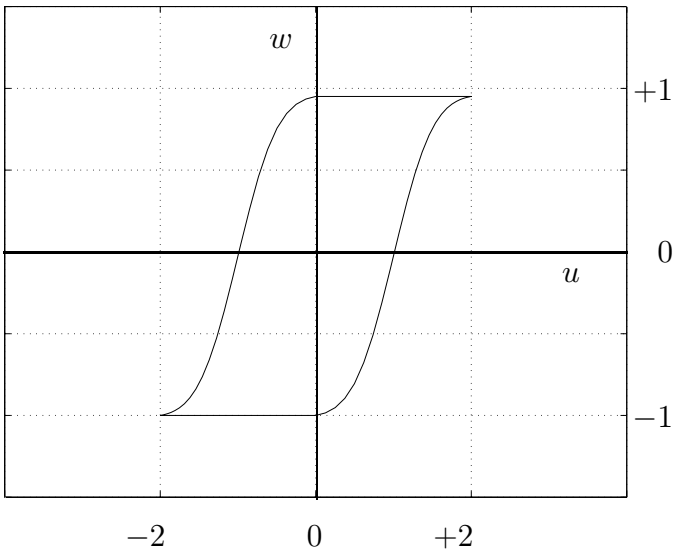

Figure 3.14: Hysteresis loop produced by simulation

and

$$\mathcal{K}_2 := \operatorname{erf}\left(\frac{\gamma}{\sqrt{2}\sigma}\right) + \operatorname{erf}\left(\frac{M_{k_t} - \gamma}{\sqrt{2}\sigma}\right).$$

3.5 Simulation

A computer simulation written in MATLAB was developed to demonstrate the capability of the inverse Preisach operator $\mathbf{P}^{-1}$ to minimize positioning error due to hysteresis. The following results are for a reference input w_d given by

$$w_d(t) = e^{-ct}\sin(2\pi\omega t + \phi).$$

When the inverse is not used to compensate for the hysteresis, the output of the actuator is given by $w(t) = [\mathbf{P}(w_d; \hat{\xi}_{k-1})](t)$.

A plot of w_d (solid line) and w (dashed line) given in Figure 3.15 shows the positioning error that results from hysteresis. Due to saturation effects of the model, a change of input direction has no effect on the output until the input crosses the line $w_d = 0$. Thus, the output $w(t)$ maintains a constant value following an input maxima or minima until $w_d = 0$. When the inverse Preisach operator $\mathbf{P}^{-1}$ is used to compensate for the hysteresis as shown in Figure 2.6 the relationship between the desired position $w_d(t)$ and the actuator output $w(t)$ becomes

$$w(t) = [\mathbf{P}(\mathbf{P}^{-1}(w_d); \hat{\xi}_{k-1})](t) = [\mathbf{P}(u^*; \hat{\xi}_{k-1})](t) = w_d(t).$$

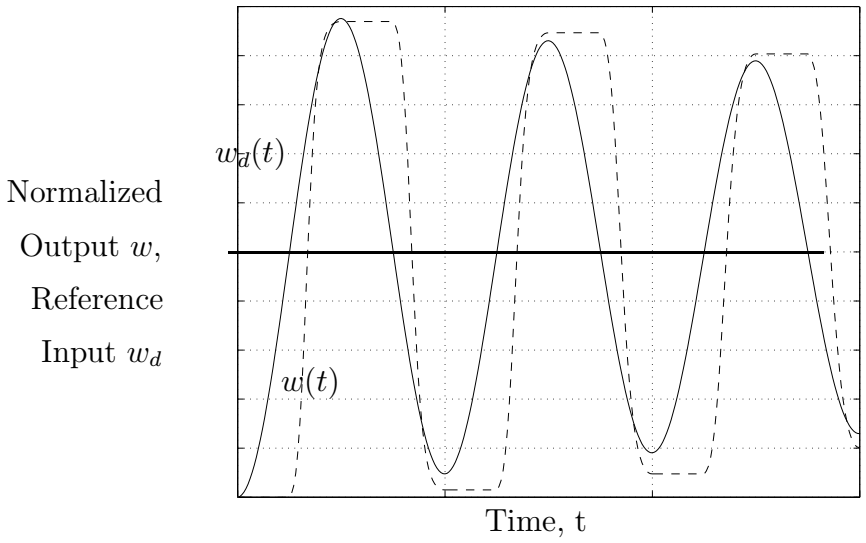

Figure 3.15: Input $w_d(t)$ (solid line) and output $w(t)$ (dashed line) for a system without compensation

The damped sine input w_d was input into $\mathbf{P}^{-1}$ and then using Equation 3.22 the compensated input u^* was computed. The input u^* is shown in Figure 3.16. Since u^* is set to zero following a local maxima or minima of w_d, the compensating input rapidly changes from its corresponding maximum or minimum. The input w^* was then input to $\mathbf{P}$ and w computed.

In Figure 3.17 the reference position input $w_d(t)$, and the output $w(t)$ are shown. As expected, for this simulation, the graphs of the two functions are indistinguishable.

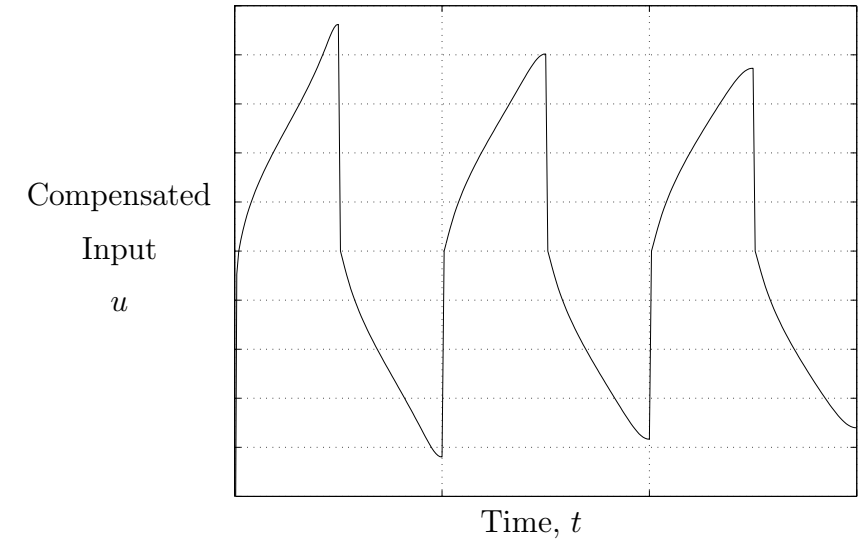

Figure 3.16: Compensating input, u^*

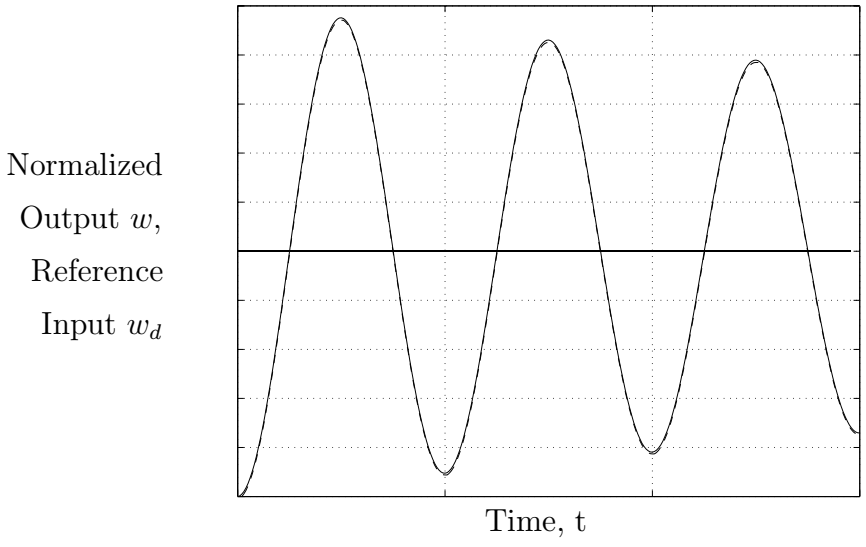

Figure 3.17: Input $w_d(t)$ and output $w(t)$ for a system with compensation

Chapter 4

The KP Operator $\mathbf{W}_{kp}$ and Inverse $\mathbf{W}_{kp}^{-1}$

Banks, Kurdila and Webb [1], [2] have developed an alternative to the Preisach operator $\mathbf{W}_{kp}$, called the KP operator. This operator is based on a generalized play type kernel (see Visintin [20]) and has similar properties to those of the Preisach operator. In this chapter, the following topics are covered:

- Description of the KP hysteresis operator $\mathbf{W_{kp}}$
- Proof that ${\mathbf{W}_{kp}}^{-1}$ exists.

4.1 Description of the KP Operator

Like the Preisach operator, the KP operator developed by Banks, Kurdila and Webb [1], [2] represents scalar hysteresis as the cummulative effect of weighted elementary hysteresis operators $\kappa_\rho(u, \xi(\rho))$ that are distributed over a domain $\rho = (\rho_1, \rho_2) \in \mathcal{P} \subseteq R^2$ called the *Preisach Plane*. Unlike the relays (used for the Preisach operator) that generate discontinuous functions on $\mathcal{P}$, the KP kernels are generalized plays (Visintin [20]) that allow the formation of continuous functions on $\mathcal{P}$.

KP Operator, $\mathbf{W}_{kp}$

For $u \in I_{u_k}$, the operators $k_\rho(u, \xi(\rho))$ map points $\rho = (\rho_1, \rho_2) \in \mathcal{P}$ to the interval $[-1, 1]$. The kernel $\kappa_\rho(u, \xi(\rho))$ used for the KP operator is given by,

$$\kappa_\rho(u, \xi_0(\rho)) = \begin{cases} max_{\rho\in\mathcal{P}}\{\xi_0(\rho), r(u, \rho_2)\} & \dot{u} > 0 \\ min_{\rho\in\mathcal{P}}\{\xi_0(\rho), r(u, \rho_1)\} & \dot{u} < 0 \end{cases}$$

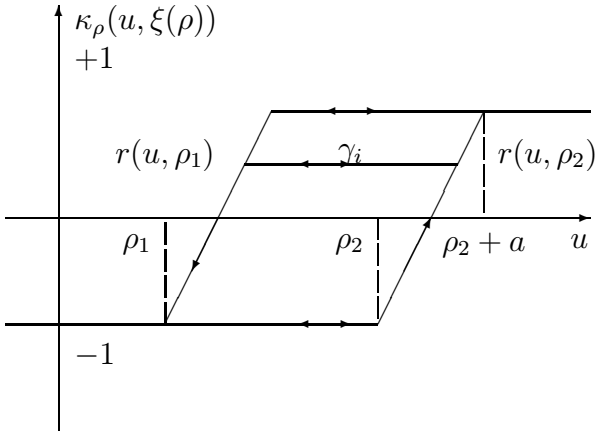

Figure 4.1: KP elementary operator

If $\dot{u} = 0$, the kernel value does not change from its previous value.

The initial value of a kernel at location ρ, is given by $\xi_0(\rho)$ where $-1 \leq \xi_0(\rho) \leq 1$. Unlike the Preisach kernel with only two branches, the KP kernel consists of a family of curves that are bounded by the curves $r(u, \rho_1)$ and $r(u, \rho_2)$ as shown in Figure 4.1. The interior paths γ_i are nonintersecting and reversible. The bounding curves join at ρ_1 and $\rho_2 + a$. Along these curves the path is not reversible for $u \in [\rho_1, \rho_1 + a]$ (decreasing) and $u \in [\rho_2, \rho_2 + a]$ (ascending). The bounding curves $r(u, \rho_1)$ and $r(u, \rho_2)$ are translates of a continuous function $r(u, x)$. This function is a continuous piecewise linear function defined as,

$$r : I_u \mathbf{x} \mathbf{R} \rightarrow [-1, 1]$$

$$r(u, x) = \begin{cases} -1 & u \leq x \\ -1 + \frac{2}{a}(u - x) & x < u < x + a \\ +1 & x + a \leq u \end{cases}$$

and is shown in Figure 4.2. The parameter "a" is greater than zero, and is chosen based on the discrete implementation. As the input u varies, the kernel output will either track along a horizontal line between the two curves $r(u, \rho_1)$ and $r(u, \rho_2)$, or along one of the two bounding curves. To illustrate this, let κ_ρ start at the intial value $\xi_0(\rho) = -1$ at time t_0 and let u vary as shown in Figure 4.3(a). As u increases, the output k_ρ follows along the lower curve $r(u, \rho_2)$. When the input starts to decrease, the output maintains the local maxima until u decreases to the point where the left curve $r(u, \rho_1)$ is intersected. The output then follows the left bounding curve until the input increases again. The output then holds at the value of the previous minima. The resulting path for the values of κ_ρ is shown in Figure 4.3(b).

KP function, ξ_u, on $\mathcal{P}$

If the input is brought to its minimum value, the kernels take on the value of -1. Starting from this initial condition, the kernel values define a function $\xi_0 : \mathcal{P} \rightarrow [-1, 1]$ equal to -1 for all points in $\mathcal{P}$, $\xi_0 \equiv 1$ on $\mathcal{P}$.

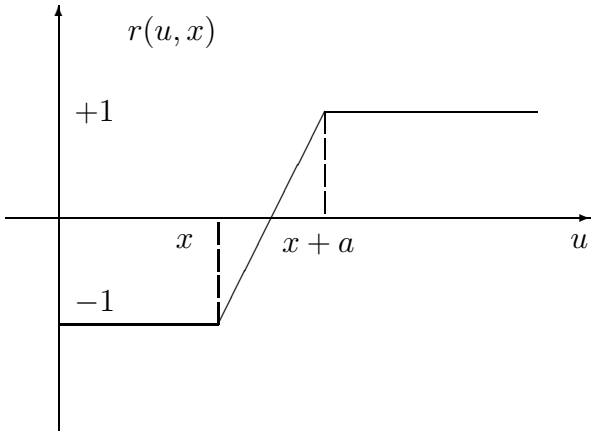

Figure 4.2: Ridge function, r(u,x)

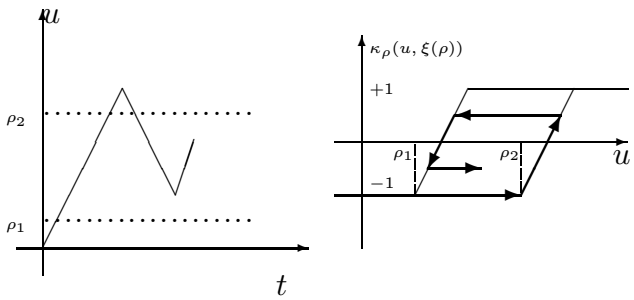

(a) $u(t)$ (b) κ_ρ

Figure 4.3: ξ_0

For the input interval $I_{u_1} = [u_0, u_1]$, a function $\xi_u : \mathcal{P} \to [-1, 1]$ on $\mathcal{P}$ is calculated for a $u \in I_{u_1}$ by the following,

$$\xi_u = \Phi(u; \xi_0)$$

where

$$\Phi : I_{u_1} \times S \to S.$$

S is the set of **continuous** measurable functions on $\mathcal{P}$, generated by the inputs $u(t) \in C_{pm}[0, T]$ and the mapping Φ. For an increasing input u in the interval I_{u_k},

$$\Phi(u; \xi_0) := max_{\rho \in \mathcal{P}}\{f_2^{kp}(u, \rho); \xi_0(\rho)\}$$

and for a decreasing input u in the interval I_{u_k},

$$\Phi(u; \xi_0) := min_{\rho \in \mathcal{P}}\{f_1^{kp}(u, \rho); \xi_0(\rho)\}$$

The two functions f_2^{kp} and f_1^{kp} are derived from the functions $r(u, \rho_1)$ and $r(u, \rho_2)$, and are defined next.

For an increasing input, the kernels define a continuous function f_2^{kp} on $\mathcal{P}$. For each value $\rho_1 \in [\mathcal{P}_{min}, \mathcal{P}_{max}]$ and $\rho_2 \in [\rho_1, P_{max}]$ the function $f_2^{kp}(u, \rho)$ maps points in $\mathcal{P}$ to the interval $[-1, 1]$,

$$f_2^{kp} : I_{u_k} \times \mathcal{P} \to [-1, 1].$$

The function $f_2^{kp}(u, \rho)$ is defined as,

$$f_2^{kp}(u, \rho) = \begin{cases} +1 & \rho_2 \leq u - a \\ -1 + \frac{2}{a}(u - \rho_2) & u - a < \rho_2 < u \\ -1 & u \leq \rho_2 \end{cases}$$

For an increasing input u the function, f_2^{kp} is translated along the ρ_2 axis. Since f_2^{kp} is continuous, u alters the kernel values smoothly from -1 to $+1$.

An example of the function f_2^{kp} for a fixed ρ_1 is shown in Figure 4.5 (a). The function f_2^{kp}, shown in Figure 4.5(b), partitions $\mathcal{P}$ into three regions. For $\rho \in \mathcal{P}^+$ the kernel values are $+1$; for $\rho \in \Delta$ the kernel values are between $+1$ and -1;for $\rho \in \mathcal{P}^-$ the kernel values are -1 (see Figure 4.4).

$f_1^{kp}(u, \rho)$ is defined in a manner similar to f_2^{kp}. For each value $\rho_2 \in [P_{min}, P_{max}]$ and $\rho_1 \in [P_{min}, \rho_2]$, we define $f_1^{kp}(u, \rho)$ as a function which maps points in $\mathcal{P}$ to the interval $[-1, 1]$,

$$f_1^{kp} : I_{u_k} \times \mathcal{P} \to [-1, 1].$$

The function $f_1^{kp}(u, \rho)$ is given by,

$$f_1^{kp}(u, \rho) = \begin{cases} +1 & \rho_1 \leq u - a \\ -1 + \frac{2}{a}(u - \rho_1) & u - a < \rho_1 < u \\ -1 & u \leq \rho_1. \end{cases}$$

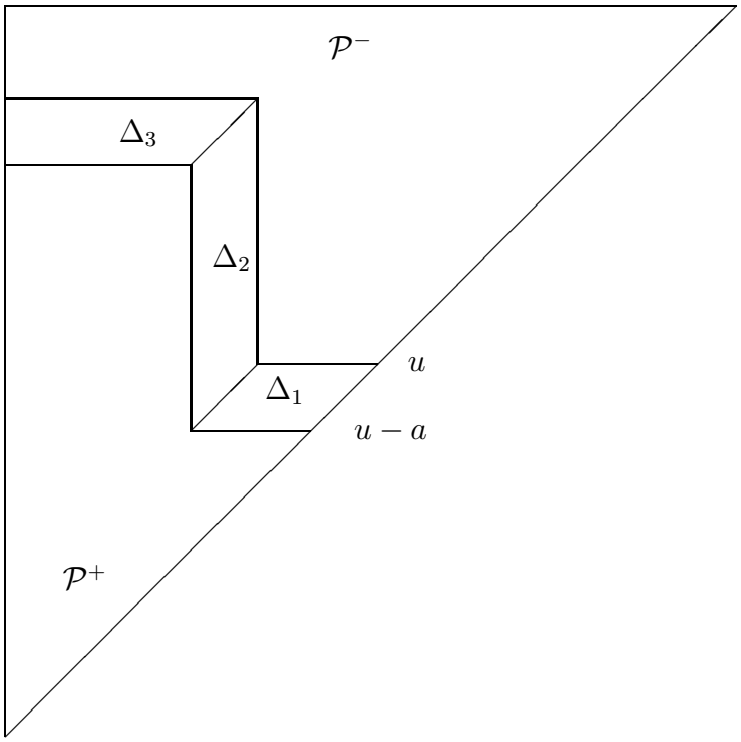

Figure 4.4: Regions of $\mathcal{P}$ for an increasing input, $\Delta = \Delta_1 \cup \Delta_2 \cup \Delta_3$

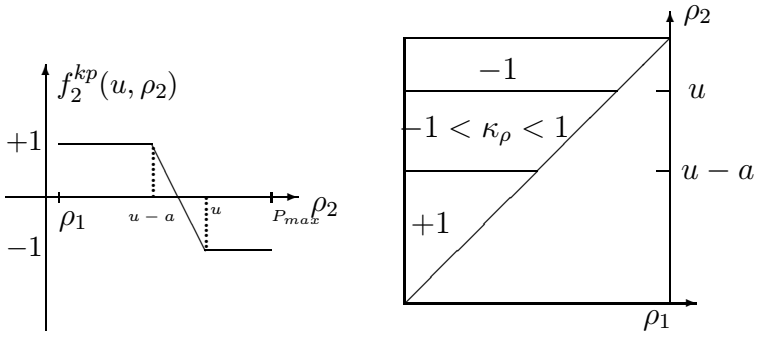

(a) $f_2^{kp}(u,\rho)$ (b) Function generated by $f_2^{kp}(u,\rho)$

Figure 4.5: Ridge function $f_2^{kp}(u,\rho)$ u increasing

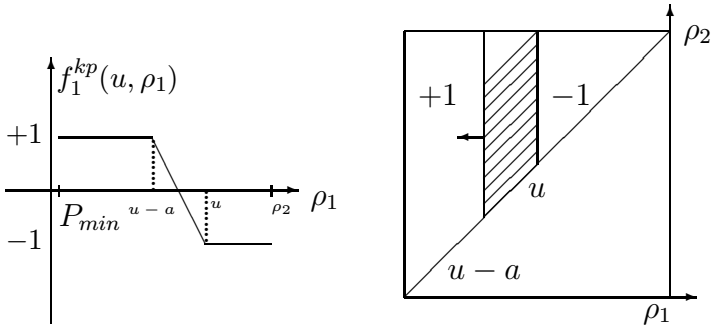

(a) $f_1^{kp}(u,\rho)$ (b) Function generated by $f_1^{kp}(u,\rho)$

Figure 4.6: Ridge function $f_1^{kp}(u,\rho)$ u decreasing

For a decreasing input u the function f_1^{kp} is translated to the left along the ρ_1 axis. An example of the function for a fixed ρ_2 is shown in Figure 4.6 (a). The continuous function $f_1^{kp}(u,\rho)$ on the Preisach plane is shown in Figure 4.6(b). For any input interval I_{u_k} the continuous function $\xi_u : \mathcal{P} \rightarrow [-1,1]$ can be calculated from u and the function ξ_{k-1} in a manner similar to that used for the Preisach operator,

$$\xi_u = \Phi(u;\xi_{k-1})$$

where

$$\xi_{k-1} = \Phi(u_{k-1};\xi_{k-2}).$$

For an increasing input u,

$$\Phi(u;\xi_{k-1}) := max_{\rho\in\mathcal{P}}\{f_2^{kp}(u,\rho),\xi_{k-1}(\rho)\}$$

and for a decreasing input u,

$$\Phi(u;\xi_{k-1}) := min_{\rho\in\mathcal{P}}\{f_1^{kp}(u,\rho),\xi_{k-1}(\rho)\}.$$

Memory and the Wiping Out Property

As with the Preisach model, the function $\xi_u : \mathcal{P} \rightarrow [-1,1]$ generated by using the KP kernel is dependent on sequences of decreasing local maximas and increasing local mimima. This is a result of the "wiping out" process described in Chapter 3. Due to the type of kernel used, there is a significant difference in the functions ξ_u that are generated.

Unlike the discontinuous function generated from the Preisach kernel, the function ξ_u generated with the KP kernel is continuous on $\mathcal{P}$. Also instead of a single curve $L(t)$ partitioning $\mathcal{P}$ into two regions $\mathcal{P}^+$ and $\mathcal{P}^-$, there is a transition region Δ where the kernel values change in a smooth manner from -1 to $+1$ on Δ. This is best shown by a simple example.

Let $u = P_{min}$ when $t = 0$. The system of kernels will be in a negative saturation state, $\xi_0(\rho) = -1$ for all $\rho \in \mathcal{P}$. As the input u increases (see Figure 4.7(a)), the state of the

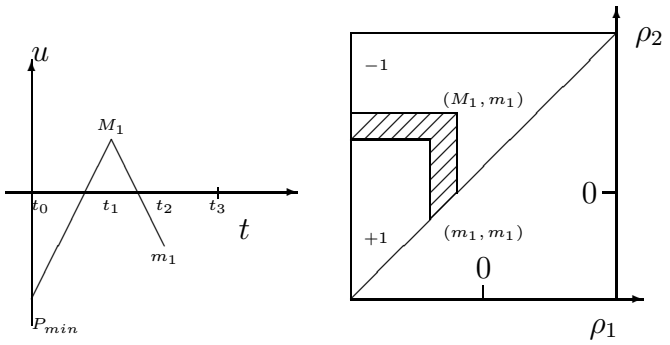

(a) $u(t)$ (b) ξ_2

Figure 4.7: ξ_2

kernels switch from -1 to +1 in a smooth fashion. Then as the input decreases over $[t_1, t_2]$ some kernels smoothly transition from $+1$ to -1. The resulting function ξ_2 is given in Figure 4.7(b). As with the Preisach model, it can be shown in general that the function ξ_u will depend on a set of decreasing local maxima $\mathcal{M}_{max}$ and the set of increasing local minima μ_{min}, as defined in Chapter 3.

4.1.1 Defining $\mathbf{W}_{kp}$ as a Composition

The KP operator for each $u \in I_{u_k}$ is now defined as the composition of an operator Φ that maps functions on the Preisach plane, to the same, and the functional Λ_μ that maps those functions to $w \in I_{w_k}$.

Define the functional Λ_μ as,

$$\Lambda_\mu(\xi_u) := \int_{\mathcal{P}} \xi_u(\rho) d\mu(\rho)$$

where Λ_μ maps the function $\xi_u : \mathcal{P} \to [-1, 1]$ to $w \in I_{w_k}$,

$$\Lambda_\mu : S \to I_{w_k}.$$

The measure μ is in $\mathcal{M}$ the set of probability measures associated with the probablity space $\{\mathcal{P}, \mathcal{B}(\mathcal{P}), \mu\}$. Due to the discontinuity of the function ξ_u and the requirement that $\mathbf{W}_{kp}$ must be a continuous function from I_{u_k} to I_{w_k}, the measure μ must be zero for vertical and horizontal lines in $\mathcal{P}$.

$$\mu(R \text{ x } \{r\}) = \mu(\{r\} \text{ x } R) = 0, \text{ for every } r \in R$$

Additionally, to maintain the strict monotonicity of the output for a strictly monotone input, the measure must be non-zero on horizontal strips, E_H, extending from a left vertical boundary given by the previous minima to the diagonal, and vertical strips, E_V, extending from the diagonal to the previous maximum of the Preisach plane (see Figure 3.12).

The KP operator $\mathbf{W}_{kp}$ is now given as a composition,

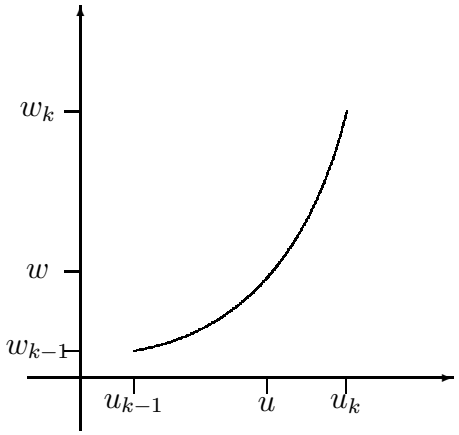

Figure 4.8: Level curve for $w = \mathbf{W}_{kp}(u; \xi_{k-1})$ with $u \in I_{u_k} = [u_{k-1}, u_k]$ increasing and $w \in I_{w_k}$

$$\mathbf{W}_{kp}(u; \xi_{k-1}) = \Lambda_\mu \circ \Phi(u; \xi_{k-1})$$

and

$$w = \mathbf{W}_{kp}(u; \xi_{k-1}).$$

$\mathbf{W}_{kp}$ is a real valued function that maps $u \in I_{u_k}$ and $\xi_u \in S$ to $w \in I_{w_k}$, and by the above composition the output w is calculated by integrating ξ_u over the Preisach plane,

$$w = \int_{\rho \in \mathcal{P}} \xi_u(\rho) d\mu(\rho). \tag{4.1}$$

An I/O curve generated by Equation 4.1 for an increasing input is shown in Figure 4.8. A similar type of curve is produced for a decreasing input. It will be shown that there is only a single curve for each interval I_{u_k}, and this fact will allow an inverse to be calculated for $\mathbf{W}_{kp}$ on intervals, I_{u_k}.

On intervals where $\dot{u}(t) \neq 0$ the function $u(t)$ is a continuous bijective function from an interval $[t_{k-1}, t_k]$ to the interval $[u_{k-1}, u_k]$ and for each time interval, $w(t) = [\mathbf{W}_{kp}(u; \xi_{k-1})](t)$. On intervals where $\dot{u}(t) = 0$, the input is constant and $u(t) = u(t_{k-1})$. The output is also constant on these intervals and $w(t) = [\mathbf{W}_{kp}(u_{k-1}, \xi_{k-1})](t)$. Therefore, with respect to each interval $[t_{k-1}, t_k]$ the KP operator, can be expressed as a mapping,

$$\mathbf{W}^{kp}(*; \xi_{k-1}) : C_{pm}[t_{k-1}, t_k] \rightarrow C_{pm}[t_{k-1}, t_k].$$

In the following discussions the time dependency is assumed and the KP operator will be discussed with respect to the input interval I_{u_k}.

4.2 $\mathbf{W}_{kp}^{-1}$

The existence of $\mathbf{W}_{kp}^{-1}$ is shown by proving that $\mathbf{W}_{kp}$ is a continuous bijective function from the interval I_{u_k} to the interval I_{w_k}.

Theorem 4.1 *The hysteresis operator, $\mathbf{W}_{kp}$ is a continuous bijective function from I_{u_k} to I_{w_k}. For $\xi_{k-1} \in S$, $I_{u_k} \ni u \rightarrow \mathbf{W}_{kp}(u; \xi_{k-1}) \in I_{w_k}$ is continuous and bijective.*

Proof: $\mathbf{W}_{kp}$ is **1-1** from I_{u_k} to I_{w_k}.

Let $u_1, u_2 \in I_{u_k}$. Assume $w_2 = w_1$ and that $u_2 > u_1$. Then,

$$\begin{aligned} 0 &= w_2 - w_1 && (4.2)\\ &= \mathbf{W}_{kp}(u_2; \xi_{k-1}) - \mathbf{W}_{kp}(u_1; \xi_{k-1}) && (4.3)\\ &= \int_{\mathcal{P}} \xi_{u_2}(\rho) - \xi_{u_1}(\rho) d\mu. && (4.4) \end{aligned}$$

The two functions differ only on the set $E \in \{E_H\}$ for u increasing or $E \in \{E_V\}$ for u decreasing. Continuing,

$$\begin{aligned} 0 &= \int_{\mathcal{P}-E} \xi_{u_2}(\rho) - \xi_{u_1}(\rho) d\mu + \int_E \xi_{u_2}(\rho) - \xi_{u_1}(\rho) d\mu && (4.5)\\ 0 &= \int_E \xi_{u_2}(\rho) - \xi_{u_1}(\rho) d\mu. && (4.6) \end{aligned}$$

Since $\xi_{u_2} - \xi_{u_1}$ is a continuous non-negative function on E, $\int_E \xi_{u_2}(\rho) - \xi_{u_1}(\rho) d\mu = 0$ only if $\xi_{u_2} = \xi_{u_1}$ except on sets of measure zero. Since it is required that, $\mu(E) > 0$, then $\xi_{u_2} = \xi_{u_1}$ on E. By the definition of ξ_u this requires $u_2 = u_1$ and so $\mathbf{W}_{kp}$ is $1-1$ from I_{u_k} to I_{w_k}.

Next it is shown that $\mathbf{W}_{kp}$ is a continuous map from I_{u_k} to I_{w_k}.

Let $\{u_n\}$ be a sequence in I_{u_k} such $u_n \rightarrow u^*$ with $u^* \in I_{u_k}$. Let $\xi_n \in S$ be the sequence of functions on $\mathcal{P}$ generated by $\xi_n = \Phi(u_n; \xi_{k-1})$ and $\xi_{u^*} = \Phi(u^*; \xi_{k-1})$, $\xi_{u^*} \in S$.

By the definition of ξ_n it can be shown that

$$\lim_{n \rightarrow \infty} \xi_n(\rho) = \xi_{u^*}(\rho)$$

for every $\rho \in \mathcal{P}$.

Let $g(\rho) = 1$, $\forall \rho \in \mathcal{P}$ then $\mid \xi_n(\rho) \mid \leq g(\rho)$. Since the functions $\xi_n \in S$ are measurable functions on $\mathcal{P}$, then

$$\lim_{n \rightarrow \infty} w_n = \lim_{n \rightarrow \infty} \int_{\mathcal{P}} \xi_n d\mu = \int_{\mathcal{P}} \xi_{u^*} d\mu = w^*$$

by the Lebesgue Convergence Theorem,

Thus for any sequence $u_n \to u^*$ in I_{u_k} we have $w_n \to w^*$. So $\mathbf{W}_{kp}$ is sequentially continuous at any u^* in I_{u_k} and $\mathbf{W}_{kp}$ is continuous on I_{u_k}.

Since $\mathbf{W}_{kp}$ is continuous and **1-1** on the closed interval I_{u_k}, $\mathbf{W}_{kp}$ is onto I_{w_k}. Thus W_{kp} is a continuous bijective function from I_{u_k} to I_{w_k}. ♣

Theorem 4.2 $\mathbf{W}_{kp} : I_{u_k} \to I_{w_k}$ *has an inverse* $\mathbf{W}_{kp}^{-1} : I_{w_k} \to I_{u_k}$.

Proof:

Since $\mathbf{W}_{kp}$ is bijective from I_{u_k} to I_{w_k}, it has a unique inverse, $\mathbf{W}_{kp}^{-1} : I_{w_k} \to I_{u_k}$. ♣

4.3 Formula for $\mathbf{W}_{kp}$

For $u \in I_{u_k}$ the KP operator can be written as follows,

$$\begin{aligned} w &= \mathbf{W}_{kp}(u; \xi_{k-1}) \\ &= \int_{\mathcal{P}} \xi_u(\rho) d\mu(\rho) \\ &= \int_{\mathcal{P}^+} \xi_u(\rho) d\mu(\rho) + \int_{\mathcal{P}^-} \xi_u(\rho) d\mu(\rho) + \int_{\Delta} \xi_u(\rho) d\mu(\rho) \\ &= \int_{\mathcal{P}^+} d\mu(\rho) - \int_{\mathcal{P}^-} d\mu(\rho) + \int_{\Delta} \xi_u(\rho) d\mu(\rho). \end{aligned} \tag{4.7}$$

For an increasing input, the delta region, Δ, is partitioned into three regions whose union equals Δ, $\Delta = \Delta_1 \cup \Delta_2 \cup \Delta_3$. Region Δ_1 is the only region that is dependent on the current input u so,

$$\begin{aligned} w &= \mu(\mathcal{P}^+) - \mu(\mathcal{P}^-) + \int_{\Delta} \xi_u(\rho) d\mu(\rho) \\ &= \mu(\mathcal{P}^+) - \mu(\mathcal{P}^-) + \int_{\Delta_1} \xi_u(\rho) d\mu(\rho) + \int_{\Delta_2 \cup \Delta_3} \xi_{k-1}(\rho) d\mu(\rho) \end{aligned} \tag{4.8}$$

where the fact that, $\xi_u = \xi_{k-1}$ on $\Delta_2 \cup \Delta_3$ if $u \leq M_k$ was used. The integral is not dependent on u directly, but only indirectly through the determination of the sets Δ_2 and Δ_3.

For increasing u on I_{u_k} the function f_2^{kp} on the region Δ_1 allows ξ_u to be defined as,

$$\xi_u(\rho_1, \rho_2) = -1 + \frac{2}{a}(u - \rho_2)$$

where $u_k - a \leq \rho_1 \leq u$. Then the first integral becomes,

$$\int_{\Delta_1} \xi_u(\rho) d\mu(\rho) = \int_{\Delta_1} -1 + \frac{2}{a}(u - \rho_2) d\mu(\rho)$$

$$
\begin{aligned}
&= -\int_{\Delta_1} d\mu(\rho) + \frac{2}{a}\int_{\Delta_1}(u-\rho_2)d\mu(\rho) \\
&= -\int_{\Delta_1} d\mu(\rho) + \frac{2}{a}u\int_{\Delta_1} d\mu(\rho) - \frac{2}{a}\int_{\Delta_1}\rho_2 d\mu(\rho) \\
\int_{\Delta_1}\xi_u(\rho)d\mu(\rho) &= -\mu(\Delta_1) + \frac{2}{a}u\mu(\Delta_1) - \frac{2}{a}\int_{\Delta_1}\rho_2 d\mu(\rho). \qquad (4.9)
\end{aligned}
$$

4.4 Formula for $\mathbf{W}_{kp}^{-1}$

Because of the continuity of ξ_u on $\mathcal{P}$, it is possible to calculate the inverse for the KP operator Starting with Equation 4.8, for $u \in I_{u_k}$, $w \in I_{w_k}$, with $\dot{u} > 0$, it can be shown that,

$$
w - \mu(\mathcal{P}^+) + \mu(\mathcal{P}^-) - \int_{\Delta_2\cup\Delta_3}\xi_{k-1}(\rho)d\mu(\rho) = \int_{\Delta_1}\xi_u(\rho)d\mu(\rho).
$$

Let $I := w - \mu(\mathcal{P}^+) + \mu(\mathcal{P}^-) - \int_{\Delta_2\cup\Delta_3}\xi_{k-1}(\rho)d\mu(\rho)$. Then using Equation 4.9,

$$
\begin{aligned}
I &= \int_{\Delta_1}\xi_u(\rho)d\mu(\rho) \\
&= -\mu(\Delta_1) + \frac{2}{a}u\mu(\Delta_1) - \frac{2}{a}\int_{\Delta_1}\rho_2 d\mu(\rho) \\
I + \mu(\Delta_1) + \frac{2}{a}\int_{\Delta_1}\rho_2 d\mu(\rho) &= u\frac{2}{a}\mu(\Delta_1) \\
\frac{\frac{a}{2}(I + \mu(\Delta_1) + \frac{2}{a}\int_{\Delta_1}\rho_2 d\mu(\rho))}{\mu(\Delta_1)} &= u \qquad (4.10) \\
\mathbf{W}_{kp}^{-1}(w) &= u.
\end{aligned}
$$

This equation gives the input $u \in I_{u_k}$ such that $\mathbf{W}_{kp}(u;\xi_{k-1}) = w$. It is important to note that to compute the inverse it is necessary to know the partitioning of the Preisach plane. If the reference input w_d is used $\mathbf{W}_{kp}^{-1}(w_d) = u^*$ and $\mathbf{W}_{kp}(u^*;\xi_{k-1}) = w_d$. A similar equation can be derived for intervals where $\dot{u} < 0$. For intervals $\dot{u} = 0$, the input is, $u = \mathbf{W}_{kp}^{-1}(w_{k-1})$.

Chapter 5

Approximations for $\mathbf{W}_{kp}$ and $\mathbf{W}_{kp}^{-1}$

The computation of the forward operator $\mathbf{W}_{kp}$ requires knowledge of the measure μ. The measure μ may be known *a priori* based on the underlying physics of the process, or it may be derived empirically from experimental data.

Two principle approaches have been used to estimate μ from data. The first is derived from a method developed by Mayergoyz [18] and demonstrated by Hughes and Wen [8] for the Preisach operator. The second approach, is the method developed by Banks, Kurdilla and Webb [1], [2], which uses discrete measures μ_n to define the approximation of the **KP** operator. The properties of the KP kernel make it possible to calculate the inverse of these discrete approximations.

In this chapter:

- An approximation, $\mathbf{W}_n$, to the hysteresis operator $\mathbf{W}_{kp}$ is developed;
- It is shown that $\mathbf{W}_n(u;\xi_{k-1}) \rightarrow \mathbf{W}_{kp}(u;\xi_{k-1})$ for $u \in I_{u_k}$ as $n \rightarrow \infty$, where $w_n = \mathbf{W}_n(u;\xi_{k-1})$;
- It is proven that the inverse $\mathbf{W}_n^{-1}(w)$ exists;
- It is shown that $\mathbf{W}_n^{-1}(w) \rightarrow \mathbf{W}_{kp}{}^{-1}(w)$.

5.1 Description of $\mathbf{W}_n$

Let $C(\mathcal{P})$ be the set of all bounded real valued continuous functions on $\mathcal{P}$, then it is possible to define a topology on the space of probability measures on $\mathcal{P}$, $\mathcal{M}(\mathcal{P})$. This is accomplished by defining a base of open neighborhoods for any measure μ in $\mathcal{M}(P)$.

Definition 5.1 *(Weak Topology on $\mathcal{M}(\mathcal{P})$) (see Bauer [26]).*

Let $\mu \in \mathcal{M}(\mathcal{P})$, then define a family of sets as follows,

$$V_\mu(f_1, f_2, \ldots, f_k; \varepsilon_1 \ldots \varepsilon_k) = \left\{\nu | \nu \in \mathcal{M}(\mathcal{P}), \left| \int_{\mathcal{P}} f_i d\nu - \int_{\mathcal{P}} f_i d\mu \right| < \varepsilon_i, i = 1, 2, \ldots, k \right\}$$

where $f_1 \ldots f_k$ are elements from $C(\mathcal{P})$ and $\varepsilon_1 \ldots \varepsilon_k$, are positive numbers. By varying k, $f_1 \ldots f_k$, and $\varepsilon_1 \ldots \varepsilon_k$, a family of sets can be generated that satisfies the axioms of a basis topology.

Within $\mathcal{M}(\mathcal{P})$ there exists a subset of "discrete" measures, μ_n, that are defined as follows.

Definition 5.2 (Discrete Measure) *The discrete probability measures μ_n on $\mathcal{P}$ are defined by,*

$$\mu_n = \sum_{i=1}^{n} \alpha_i \delta_{x_i}$$

where $x_1, \ldots, x_n \in \mathcal{P}$ and $\alpha_i \geq 0$ with $\sum_{i=1}^n \alpha_i = 1$. δ_{x_i} is the Dirac measure with atom at x_i. If $x_i \in E \subset \mathcal{P}$ then $\delta_{x_i} = 1$, otherwise $\delta_{x_i} = 0$.

The set of all such discrete measures on $\mathcal{P}$ is $\mathcal{M}_D(\mathcal{P})$. To be able to approximate μ with μ_n it is necessary that the set of discrete measures is dense in $\mathcal{M}(\mathcal{P})$.

Theorem 5.1 *$\mathcal{M}_\mathcal{D}(\mathcal{P})$ is dense in $\mathcal{M}(\mathcal{P})$.*

Proof: Use the weak topology on $\mathcal{M}(P)$ as defined above. It is necessary to show that for any open set containing μ, it also contains a μ_n. To begin, let $\mu \in V_\mu$. The Preisach plane $\mathcal{P}$ is a separable metric space (rationals countable and dense in $\mathcal{P}$). Since $\mathcal{P}$ is separable, for each integer n, the sets A_j are chosen so that $\mathcal{P} = \cup_{j=1}^n A_j$, and $A_j \cap A_k = \emptyset$ if $j \neq k$, $A_j \in \mathcal{B}(\mathcal{P})$. The "diameter" of each set A_j is $\leq 1/n$ for all j. Let μ_n be the measure with masses $\mu(A_j)$ at the points ρ_j, in A_j. Let $f \in C(\mathcal{P})$.

Let $y_j = \sup_{\rho \in A_j}(f(\rho))$ and $l_j = \inf_{\rho \in A_j}(f(\rho))$. Then

$$\begin{aligned}
\left| \int_{\mathcal{P}} f d\mu_n - \int_{\mathcal{P}} f d\mu \right| &= | \sum_{j=1}^{n} \int_{A_j} (f(\rho_j) - f(\rho)) d\mu | && (5.1)\\
&\leq \sum_{j=1}^{n} \int_{A_j} | (f(\rho_j) - f(\rho)) | d\mu && (5.2)\\
&\leq \sum_{j=1}^{n} (y_j - l_j) \int_{A_j} d\mu && (5.3)\\
&\leq \sup_j (y_j - l_j) \sum_{j=1}^{n} \int_{A_j} d\mu && (5.4)\\
&\leq \sup_j (y_j - l_j). && (5.5)
\end{aligned}$$

By making n large enough the right side can be reduced so that,

$$\left| \int_{\mathcal{P}} f d\mu_n - \int_{\mathcal{P}} f d\mu \right| \leq \sup_j (y_j - l_j) \leq \epsilon.$$

The above holds for any $\epsilon > 0$ and for and all $f \in C(\mathcal{P})$. Thus there is a μ_n in every open set containing μ. Therefore $\mathcal{M}_{\mathcal{D}}$ is dense in $\mathcal{M}$. ♣

Thus for each measure $\mu \in \mathcal{M}(P)$ there exists a discrete measure $\mu_n \in \mathcal{M}(\mathcal{P})$ that can be used to approximate μ with any accuracy that is required.

5.1.1 $\mathbf{W}_n$ an Approximation of $\mathbf{W}_{kp}$

An approximation to $\mathbf{W}_{kp}$ is obtained by using a discrete measure $\mu_n \in \mathcal{M}_{\mathcal{D}}(\mathcal{P})$ to approximate the measure μ. The approximation $\mathbf{W_n}$ is given by

$$\begin{aligned} \mathbf{W}_n(u; \xi_{k-1}) &= \Lambda_n \circ \Phi(u; \xi_{k-1}) && (5.6) \\ &= \Lambda_n(\xi_u) && (5.7) \\ &= \int_{\mathcal{P}} \xi_u(\rho) d\mu_n && (5.8) \end{aligned}$$

where ξ_{k-1} represents the initial state of the KP kernels on the Preisach plane for $u \in I_{u_k}$, and Λ_n is given by,

$$\Lambda_n(\xi_u) := \int_{\rho \in P} \xi_u(\rho) d\mu_n(\rho).$$

Like $\mathbf{W}_{kp}$, $\mathbf{W}_n(u; \xi_{k-1})$ is a real valued function that maps $u \in I_{u_k}$ to $w \in I_{w_k}$. Since $\mathbf{W}_{kp}$ is a continuous bijective function from I_{u_k} to I_{w_k}, then so is $\mathbf{W}_n$. By the same argument, $\mathbf{W}_n : C_{pm}[0,T] \to C_{pm}[0,T]$. Next it is shown that as n increases the sequence of approximations $\{\mathbf{W}_n\}$ converge uniformly to $\mathbf{W}_{kp}$ on I_{u_k}.

Theorem 5.2 *$\mathbf{W}_n(u; \xi_{k-1})$ converges to $\mathbf{W}(u; \xi_{k-1})$ on I_{u_k} as $n \to \infty$.*

Proof:
Choose $\mu \in \mathcal{M}(\mathcal{P})$. Since $\mathcal{P}$ is separable, for each integer n, it can be partitioned into n sets where $\mathcal{P} = \bigcup_j A_{nj}$, $A_{nj} \bigcap A_{nk} = \emptyset$ if $j \neq k$, $A_{nj} \in \mathcal{B}(\mathcal{P})$ for all n and j, and the "diameter" of A_{nj} is $\leq 1/n$ for all j. Let $\rho_{nj} \in A_{nj}$ and μ_n is a measure with masses $\mu(A_{nj})$ at the points ρ_{nj}. Let $\xi_u \in S \subset C(\mathcal{P})$ and

$$l_{nj} = \inf_{\rho \in A_{nj}} \xi_u(\rho)$$

and

$$y_{nj} = \sup_{\rho \in A_{nj}} \xi_u(\rho).$$

For $u \in I_{u_k}$

$$\begin{aligned} \mid \mathbf{W}_n(u;\xi_{k-1}) - \mathbf{W}(u;\xi_{k-1}) \mid &= \mid \int \xi_u d\mu_n - \int \xi_u d\mu \mid & (5.9)\\ &= \mid \sum \int_{A_{nj}} (\xi_u(\rho_{nj}) - \xi_u(x)) d\mu \mid & (5.10)\\ &\leq \mid \sup_j (y_{nj} - l_{nj}) \sum_j \mu(A_{nj}) \mid & (5.11)\\ &\leq \mid \sup_j (y_{nj} - l_{nj}) \mid . & (5.12) \end{aligned}$$

As $n \to \infty$ the diameter of $A_{nj} \to 0$ then $\sup_j (y_{nj} - l_{nj}) \to 0$, and so $\mathbf{W}_n \to \mathbf{W}$ for every $u \in I_{u_k}$ given $\xi_{k-1} \in S$. ♣

Previously, for the operator $\mathbf{W}_{kp}(u;\xi_{k-1})$ and an increasing input, it was shown that,

$$w = \mu(\mathcal{P}^+) - \mu(\mathcal{P}^-) + \int_{\Delta_1} \xi_u(\rho) d\mu(\rho) + \int_{\Delta_2 \cup \Delta_3} \xi_{k-1}(\rho) d\mu(\rho).$$

Using the discrete measure μ_n, the output of the approximation, $w_n = \mathbf{W}_n(u;\xi_{k-1})$, is given by

$$w_n = \mu_n(\mathcal{P}^+) - \mu_n(\mathcal{P}^-) + \int_{\Delta_1} \xi_u(\rho) d\mu_n(\rho) + \int_{\Delta_2 \cup \Delta_3} \xi_{k-1}(\rho) d\mu_n(\rho). \quad (5.13)$$

For the function f_2^{kp} on the region Δ_1 , ξ_u is defined as,

$$\xi_u(\rho_1, \rho_2) = -1 + \frac{2}{a}(u - \rho_2)$$

where ρ_1 takes on all values $u_k - a \leq \rho_1 \leq u$. Then,

$$\int_{\Delta_1} \xi_u(\rho) d\mu_n(\rho) = -\mu_n(\Delta_1) + \frac{2}{a} u \mu_n(\Delta_1) - \frac{2}{a} \int_{\Delta_1} \rho_2 d\mu_n(\rho).$$

A similar result can be found for a decreasing input $\dot{u} < 0$. For the case where $\dot{u} = 0$, w_n is equal to the previous output value.

5.2 $\mathbf{W}_n^{-1}$

The inverse $\mathbf{W}_{kp}^{-1}$ exists for all $\mu \in \mathcal{M}(\mathcal{P})$, and since $\mu_n \in \mathcal{M}_D(\mathcal{P}) \subset \mathcal{M}(\mathcal{P})$, $\mathbf{W}_n$ has an inverse, $\mathbf{W}_n^{-1}$. The inverse approximation is obtained by using the formula for $\mathbf{W}_{kp}^{-1}$ and the discrete measure μ_n. This leads to the following formula for u_n,

$$\begin{aligned} \frac{\frac{a}{2}(I_n + \mu_n(\Delta_1) + \frac{2}{a}\int_{\Delta_1} \rho_2 d\mu_n(\rho))}{\mu_n(\Delta_1)} &= u_n & (5.14)\\ \mathbf{W}_n^{-1}(w) &= u_n \end{aligned}$$

where $w \in I_{w_k}$, and I_n is given by

$$I_n := w - \mu_n(\mathcal{P}^+) + \mu_n(\mathcal{P}^-) - \int_{\Delta_2 \cup \Delta_3} \xi_{k-1}(\rho) d\mu_n(\rho).$$

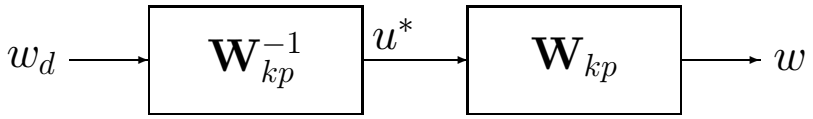

Figure 5.1: Open loop control of an actuator with hysteresis

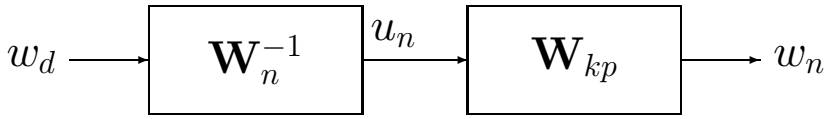

Figure 5.2: Open loop control using inverse approximation

5.2.1 Convergence, $u_n \to u^*$

The original model for an open loop compensation system is shown in Figure 5.1. To determine u^* it is necessary that $\mathbf{W}_{kp}$ accurately model the hysteresis and that an inverse ${\mathbf{W}_{kp}}^{-1}$ can be determined. Since μ is unknown, $\mathbf{W}_{kp}^{-1}$ is replaced with the inverse of the approximation, $\mathbf{W}_{n}^{-1}$, as shown in Figure 5.2. For the approximation to produce the desired identity map (so that $w_d = w$) it is necessary that $u_n \to u^*$ as $n \to \infty$, where $u_n = \mathbf{W}_{n}^{-1}(w)$ and $u^* = \mathbf{W}_{kp}^{-1}(w)$, for every $w \in I_{w_k}$.

Theorem 5.3 *$u_n \to u^*$, $\mathbf{W}_{n}^{-1}(w)$ converges to $\mathbf{W}^{-1}(w)$ for every $w \in I_{w_k}$.*

Proof:
Weak Convergence Let $\mu \in \mathcal{M}(\mathcal{P})$, $f \in \mathcal{C}(\mathcal{P})$, and $E \in \mathcal{B}(\mathcal{P})$. For each integer n, the sets A_j are chosen so that $E = \cup_{j=1}^{n} A_j$, $A_j \cap A_k = \emptyset$ if $j \neq k$. The "diameter" of each set A_j is $\leq 1/n$ for all j. Let μ_n be a measure with masses $\mu(A_j)$ at the points ρ_j in the A_j. Let $y_j = \sup_{\rho \in A_j}(f(\rho))$ and $l_j = \inf_{\rho \in A_j}(f(\rho))$. Then

$$\left| \int_E f d\mu_n - \int_E f d\mu \right| = | \sum_{j=1}^{n} \int_{A_j} (f(\rho_j) - f(\rho)) d\mu | \tag{5.15}$$

$$\leq \sum_{j=1}^{n} \int_{A_j} | (f(\rho_j) - f(\rho)) | d\mu \tag{5.16}$$

$$\leq \sum_{j=1}^{n} (y_j - l_j) \int_{A_j} d\mu \tag{5.17}$$

$$\leq \sup_j (y_j - l_j) \sum_{j=1}^{n} \int_{A_j} d\mu \tag{5.18}$$

$$\leq \sup_j (y_j - l_j) \mu(E). \tag{5.19}$$

As $n \to \infty$ the diameter of the sets $A_j \to 0$, leading to

$$\left| \int_E f d\mu_n - \int_E f d\mu \right| \to 0$$

Thus μ_n converges weakly to μ. Weak convergence is designated by $\mu_n \Rightarrow \mu$.

For each term in Equation 5.14, as $n \to \infty$ by weak convergence we have,

$$\begin{aligned} \mu_n(\mathcal{P}^+) &\to \mu(\mathcal{P}^+) \\ \mu_n(\mathcal{P}^-) &\to \mu(\mathcal{P}^-) \\ \int_{\Delta_2 \cup \Delta_3} \xi_u(\rho) d\mu_n(\rho) &\to \int_{\Delta_2 \cup \Delta_3} \xi_u(\rho) d\mu(\rho) \end{aligned}$$

so, $I_n \to I$. Also,

$$\begin{aligned} \frac{2}{a} \int_{\Delta_1} \rho_2 d\mu_n(\rho) &\to \frac{2}{a} \int_{\Delta_1} \rho_2 d\mu(\rho) \\ \mu_n(\Delta_1) &\to \mu(\Delta_1) \end{aligned}$$

and using Equations 4.11 and 5.14 it is shown that $u_n \to u^*$. ♣

For $w = w_d$, the input generated by the inverse of the approximation $u_n = \mathbf{W}_n^{-1}(w_d)$ converges to the input $u^* = \mathbf{W}_{kp}{}^{-1}(w_d)$ and the desired identity map is obtained.

It is important to note that the convergence relies on the form of the function ξ_u. The continuity of ξ_u and the fact that u enters into the function explicitly, allows the inverse to be determined. These two properties were not available for the Preisach operator since the relay kernel generates a discontinuous function on $\mathcal{P}$. Therefore, it is not possible to calculate a similar inverse for $\mathbf{P}$.

5.2.2 $\mathbf{W}_n^{-1}$ Formulation using Discrete Measure

Since $\mathcal{P}$ is separable, it can be partitioned into n sets A_j, where $\mathcal{P} = \bigcup_{j=1}^{n} A_j$, $A_j \bigcap A_k = \emptyset$ if $j \neq k$, $A_j \in \mathcal{B}(\mathcal{P})$ for all n and j. Let $\rho_j \in A_j$ and as before μ_n is a measure with masses $\mu(A_j)$ at the points ρ_j.

Let $\alpha_j = \mu(A_j)$ and let them be located at the point ρ_j in the Preisach plane. A computational form for the approximation $\mathbf{W}_n(u;\xi_{k-1})$ can be derived as follows,

$$w_n = \mu_n(\mathcal{P}^+) - \mu_n(\mathcal{P}^-) + \int_\Delta \xi_u(\rho) d\mu_n(\rho) = \sum_{\rho_j \in \mathcal{P}} \alpha_j \xi_u(\alpha_j) \tag{5.20}$$

Let the sets A_j and the nodes ρ_j be chosen, so that the ρ_j are equally spaced on $\mathcal{P}$ and rational. This will produce a grid pattern on $\mathcal{P}$. A formula for $\mathbf{W}_n^{-1}$ is now derived, for $\dot{w}_d \neq 0$. Remember it is our goal to find an input u^* so that $w(t) = w_d(t)$ for $t \in [t_{k-1}, t_k]$. Using this equality it follows that a change in the reference,

$$\Delta w_d = w_d(t) - w_d(t_0)$$

is equal to a change in the output

$$\Delta w = w(t) - w(t_0).$$

This gives the following result,

$$\begin{aligned} \Delta w_d &= \Delta w & (5.21)\\ &= \mathbf{W}_n(u;\xi_{k-1}) - \mathbf{W}_n(u_0;\xi_{k-1}) & (5.22)\\ &= \sum_{j=1}^{n} (\xi_u(\rho_j) - \xi_{u_0}(\rho_j))\alpha_j. & (5.23) \end{aligned}$$

The difference between the functions ξ_u and ξ_{u_0} is zero except on a set E_H for $\dot{w} > 0$ or a set E_V for $\dot{w} < 0$. Additionally, if the change in the reference Δw_d is chosen so that $\mid u - u_0 \mid$ is less than the distance between two adjacent nodes, then

$$\xi_u(\rho_j) - \xi_{u_0}(\rho_j) = \tfrac{2}{a}(u - u_0).$$

This gives us,

$$\Delta w_d = \textstyle\sum_{\rho_j \in E_H, E_V} \frac{2}{a}(u - u_0)\alpha_j.$$

and solving for u, we obtain

$$u = \frac{\frac{a}{2}\Delta w_d}{\sum_{\rho_j \in E_H, E_V} \alpha_j} + u_0 \tag{5.24}$$

Thus,

$$\mathbf{W}_n^{-1}(w_d) := \frac{\frac{a}{2}\Delta w_d}{\sum_{\rho_j \in E_H, E_V} \alpha_j} + u_0. \tag{5.25}$$

Chapter 6

Computer Simulation using the KP Operator

In this chapter, the capabilites of $\mathbf{W}_n$ and $\mathbf{W}_n^{-1}$ are demonstrated through the use of a computer simulation. This demonstration includes the following:

- Generation of simulation data;
- Identification of α_i;
- Estimation of w using forward operator $\mathbf{W}_n$;
- Estimation of u^* using inverse operator $\mathbf{W}_n^{-1}$.

6.1 Simulation Data

It is first demonstrated that the forward model $\mathbf{W}_n$ generates scalar hysteresis loops. Demonstrating this requires the specification of the weights, α_i, and an input u. The parameters α_i are weighting values distributed over the Preisach plane, and the shape of their distribution determines the shape of the corresponding I/O curves. In this demonstration, a bivariate distribution similar to a bivariate normal density is used to specify the weights. The process consists of first computing,

$$\gamma(\rho_1, \rho_2) = c_1 * e^{c_2((\rho_1-\bar{\rho}_1)^2+(\rho_2-\bar{\rho}_2)^2)}$$

where the constants are given by $c_1 = \frac{1}{2\pi\sigma^2}$, $c_2 = \frac{1}{2\sigma^2}$, $\sigma = 0.6$, and $\bar{\rho}_1 = \bar{\rho}_2 = 0$. The constant σ specifies the spread of the distribution, and the means of $\bar{\rho}_1, \bar{\rho}_2$ are the center of the distribution.

0.00000										
0.00001	0.00010									
0.00006	0.00046	0.00218								
0.00019	0.00140	0.00663	0.02013							
0.00037	0.00272	0.01291	0.03921	0.07637						
0.00046	0.00340	0.01612	0.04897	0.09538	0.11911					
0.00037	0.00272	0.01291	0.03921	0.07637	0.09538	0.07637				
0.00019	0.00140	0.00663	0.02013	0.03921	0.04897	0.03921	0.02013			
0.00006	0.00046	0.00218	0.00663	0.01291	0.01612	0.01291	0.00663	0.00218		
0.00001	0.00010	0.00046	0.00140	0.00272	0.00340	0.0272	0.00140	0.00046	0.00010	
0.00000	0.00001	0.00006	0.00019	0.00037	0.00046	0.00037	0.00019	0.00006	0.00001	0.0000

Table 6.1: α_i for bivariate distribution $\bar{\rho}_1 = 0$ and $\bar{\rho}_2 = 0$, $\sigma = .6$

The α_i are calculated by normalizing the γ values so that the weights sum to a value of 1.

$$\alpha_i = \frac{\gamma(\rho_i)}{\sum_{i=1}^{n} \gamma(\rho_i)} \text{ where } i = 1, \ldots, n$$

For this example, sixty six parameter values were calculated, $n = 66$. The α_i are listed in Table 6.1. The values are ordered from left to right, starting with the top row. This ordering gives $\alpha_1 = 0.0000$, $\alpha_2 = 0.00001$, $\alpha_3 = 0.00010$ and so forth. The α_1 value is located at the lower left node in the Preisach plane.

A sinusoidal input (shown in Figure 6.1) and the above parameters were used with the approximation formula $\mathbf{W}_n$,

$$w = \mathbf{W}_n(u; \xi_{k-1}) = \sum_{j=1}^{66} \xi_u(\rho_j)\alpha_j$$

to compute a sequence of output values w. The resulting data (u, w) is plotted in Figure 6.2. The I/O curves show the S-type of hysteresis curves generated by the bivariate distribution function and is often observed in the magnetic recording industry. Thus, it has been shown that the operator $\mathbf{W}_n$ is capable of generating scalar hysteresis curves.

6.2 The Parameter Identification Process

In the preceeding section, the parameters α_i were given and the data (u, w) were computed. In this section, the I/O data (u, w) is given and the α_i parameters are estimated from the data. In this case, the data (u, w) is the data generated by the procedure described above. The α_i parameters are estimated by using a nonnegative least squares algorithm found in MATLAB. The resulting estimated parameter values, $\hat{\alpha}_i$, are given in Table 6.2.

The two tables for α_i and $\hat{\alpha}_i$ differ slightly for all entry values except for the last row. In that row, the values are concentrated at one node, $\hat{\alpha}_{56} = 0.00170$. This value is near the sum of the values (0.00172) in the last row of the α_i data. It appears that the α_i weights of

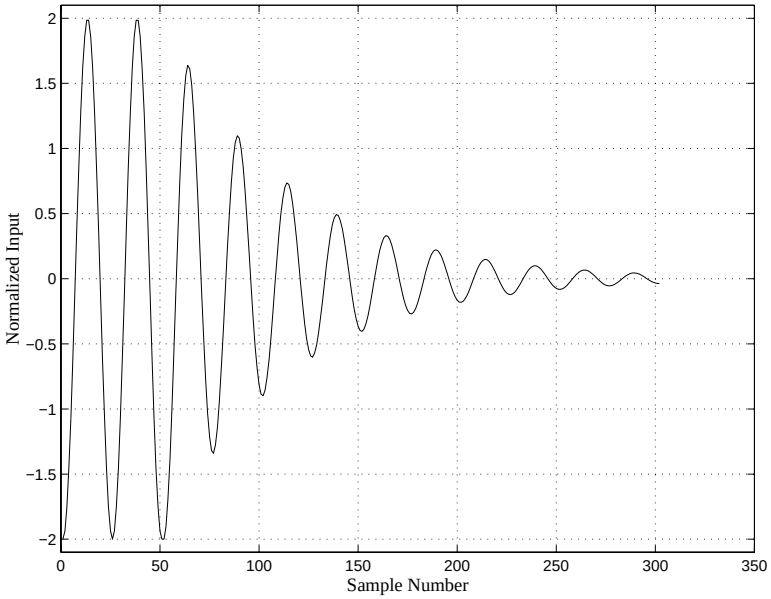

Figure 6.1: Bivariate sine input, u

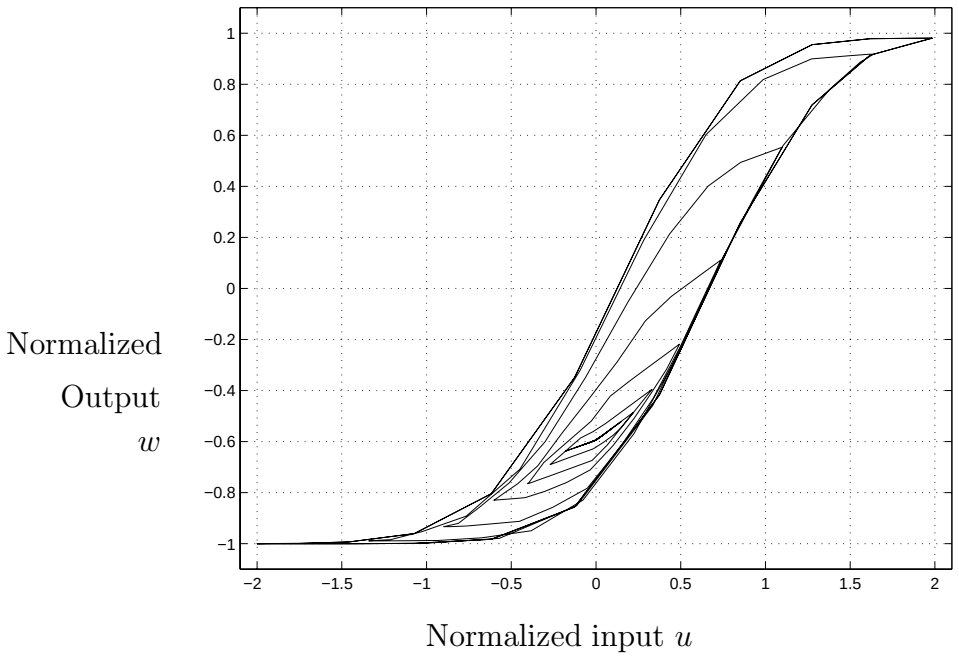

Figure 6.2: Bivariate input and output (u, w)

0.00000										
0.00000	0.00012									
0.00000	0.00054	0.00215								
0.00020	0.00150	0.00652	0.02017							
0.00039	0.00267	0.01282	0.03932	0.07633						
0.00048	0.00336	0.01619	0.04906	0.09527	0.11915					
0.00040	0.00266	0.01297	0.03914	0.07629	0.09549	0.07634				
0.00024	0.00130	0.00671	0.02007	0.03928	0.04906	0.03910	0.02017			
0.00000	0.00048	0.00226	0.00654	0.01297	0.01605	0.01282	0.00674	0.00215		
0.00002	0.00015	0.00043	0.00132	0.00280	0.00334	0.0280	0.00149	0.00035	0.00013	
0.00170	0.00000	0.00000	0.00000	0.00000	0.00000	0.00000	0.00000	0.00000	0.00000	0.0000

Table 6.2: Estimates for bivariate distribution, $\hat{\alpha}_i$

the last row are concentrated at the single node. This is a result of the input function not reaching the maximum and minimum output values.

The type of input used to identify the parameters is important. After some empirical testing, it was discovered that the damped sinusoidal input u, used above, allowed for the recovery of the majority of the α_i values. Other types of input functions resulted in sparse matrices with the sum of the row or column weights concentrated at single nodes. In future work the amount and type of training data should be resolved. It appears that there should be an optimal input function for estimating the weights.

6.3 Estimation of w using the Forward Operator $\mathbf{W}_n$.

To demonstrate the accuracy of the forward model, the parameters identified in the previous section were used to generate a typical hysteresis output. The input, shown in Figure 6.3, was used to generate the two outputs $\hat{w}$ and w. The $\hat{w}$ output used the estimated $\hat{\alpha}_i$ parameters and the output w was generated using the true α_i parameters. The two outputs, shown in Figure 6.4, are similar for the given input. The maximum error between $\hat{w}$ and w is less than $1\text{x}10^{-05}$. Based on this example, it appears that $\mathbf{W}_n$ accurately models $\mathbf{W}$ for the simulation.

6.4 Estimation of u^* using the Inverse Operator $\mathbf{W}_n^{-1}$

As shown in Figure 6.5, the reference signal w_d is used to generate an input u_n that provides compensation for hysteresis. If u_n is near the optimal input, u_* then $w_n \approx w_d$.

A cyclic reference w_d (see Figure 6.6) is used to generate a compensation input, u_n by the formula $u_n = \mathbf{W}_n^{-1}(w_d)$. A plot of the resulting u_n is shown in Figure 6.7. The flat regions of u_n correspond to small variations in w_d (a small change in w_d is < 0.00001). This is important since flat regions of the reference imply infinite inputs u_n, so the input must be held constant when this occurs.

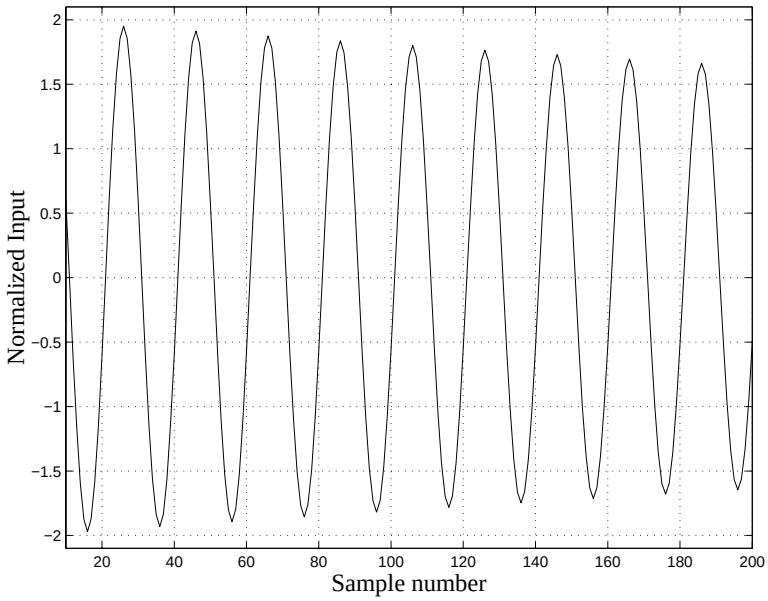

Figure 6.3: Simulation input u

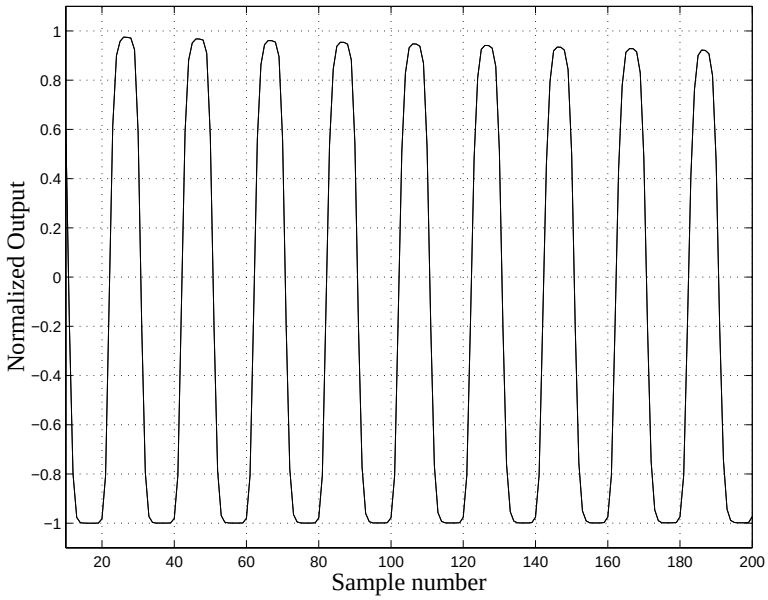

Figure 6.4: Output w_n, reference input w_d and error $w_d - w_n$ generated with $\hat{\alpha}_i$ and α_i

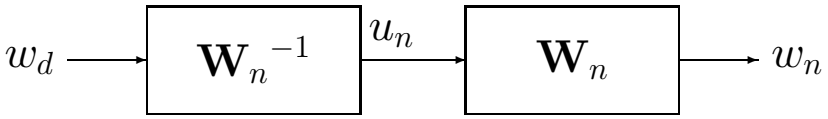

Figure 6.5: Open loop control of an actuator with hysteresis

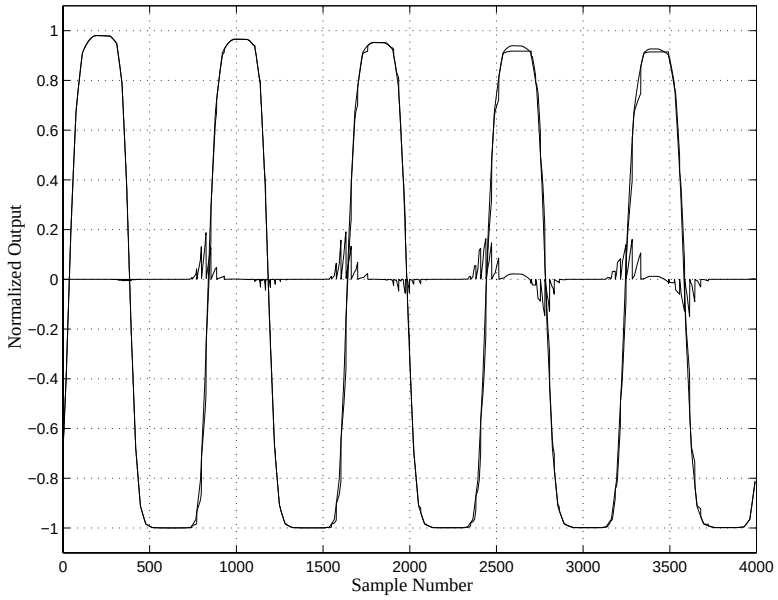

Figure 6.6: Outputs $\hat{w}$ and w generated with $\hat{\alpha}_i$ and inverse $\hat{u^*}$

Figure 6.6 is a plot of a reference input w_d, the the simulation output w_n generated by using u_n as input, and the error between the two, $e = w_d - w_n$. The error is nearly zero for the first cycle indicating that the compensating input is removing the majority of the hysteresis effect. However, after the first cycle, the error exhibits a sequence of sawtooth oscillations during increasing and decreasing inputs. Because the initial cycle is free from this error it is suspected that the simulation code contains an error.

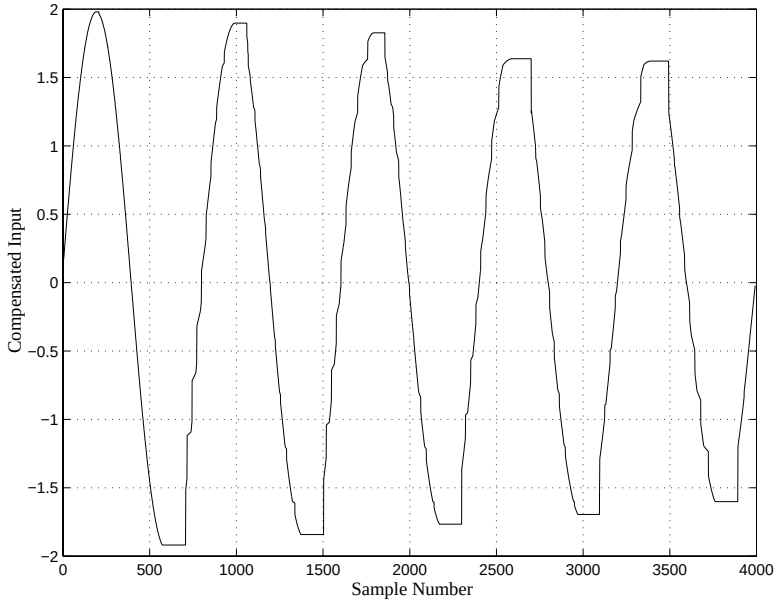

Figure 6.7: Input u_n generated by $u_n = \mathbf{W}_n^{-1}(w_d)$

Chapter 7

Experimental Results for the KP Operator

Data collected from an actuator with scalar hysteresis was used to test the accuracy of the forward model $\mathbf{W}_n$, and to test the feasibility of using the inverse $\mathbf{W}_n^{-1}$ to provide the compensation necessary to reduce the postitioning error created by hysteresis.

In this chapter the following topics are discussed;

- Experimental Data;
- Parameter Identification, α_i;
- Estimation of w using forward operator $\mathbf{W}_n$;
- Estimation of u^* using inverse operator $\mathbf{W}_n^{-1}$.

7.1 Experimental Data

The experimental setup, shown in Figure 7.1, was used to record the input voltages and tip displacements of an unloaded Physik piezoelectric stack. A function generator was used to produce a negatively offset sinusoidal signal with amplitudes in the range of 0 to -10 Volts at a frequency of 0.05 Hz. This signal was input into a power amplifier that generated a sinusoidal voltage between 0 and -1000 Volts for input to the stack. At the other end of the stack, a fiber optic displacement sensor was used to measure the displacement of the stack resulting from the varying input voltage.

Input and displacement data were recorded for 3 voltage ranges. The three voltage ranges were; 0 to -803 volts, D800; 0 to -643 volts, D600; 0 to -426 volts D400. The voltage ranges

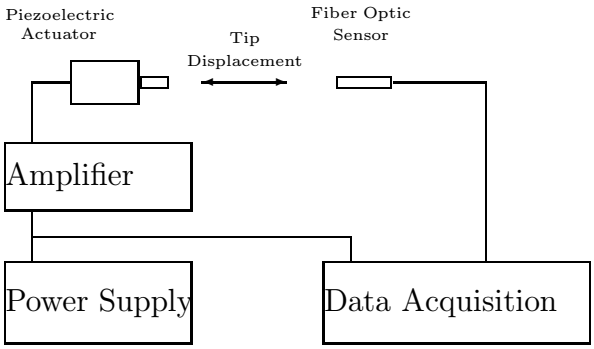

Figure 7.1: Experimental Setup

Label	Voltage Range
D800	0 to -803 Volts
D600	0 to -643 Volts
D400	0 to -426 Volts

Table 7.1: Input Voltage Ranges for the Data Sets

and labels for each data set are given in Table 7.1. A data sample set consists of the pair (u, w), where u is the output voltage from the function generator and w is the output voltage from the displacement sensor.

Both outputs were sampled at 12.8 Hz and 1024 sample pairs were recorded from each. This corresponds to 80 seconds of data or approximately 4 voltage cycles of the input. The two measurements were scaled so that u ranges from -2 to 2 and w ranges from -1 to $+1$. A plot of w versus u for samples from the three data sets is shown in Figure 7.2.

The plot shows three hysteresis loops. The D800 data is the largest loop and will be considered the major hysteresis loop, while the two inner loops formed by the D600 and D400 data respectively. The scalar hysteresis of the actuator is evident in the graph.

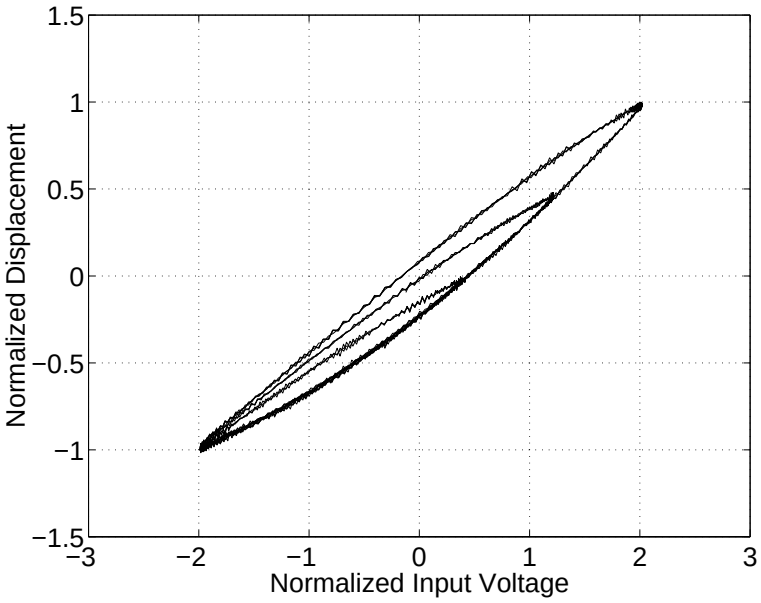

Figure 7.2: D800, D600, D400 I/O

7.2 Parameter Identification

The parameters α_i of $\mathbf{W}_n$ were identified using a subset of the major loop data (D800) and a nonnegative least squares approximation (NNLS in MATLAB). The resulting parameter estimates α_i are given in Table 7.2 for fifty five nodes, n=55. The table is organized so that the upper left element corresponds to the first node in the lower left corner of the Preisach plane. This ordering gives $\alpha_1 = 0.1210$, $\alpha_2 = 0.0232$, $\alpha_3 = 0.0237$ and so on.

Two prominent features are observed in Table 7.2. The first is that some rows and columns contain zeros for the majority of the nodes. As in the simulation data, this occurs when the training set is insufficient to recover the individual α_i parameters, but is sufficient enough to obtain a column or row sum value. Secondly, the diagonal has three values that are zero. At these turning points there will be no change in the output for a change in the input. If this happens, the inverse calculation generates an infinite input, u. To compensate for this, the algorithm was modified to use the previous input as the current input. Thus for no change in w, there is no change in u.

0.1210									
0.0232	0.0237								
0.00000	0.0	0.1083							
0.0	0.0	0.0374	0.0816						
0.0	0.0	0.0338	0.0	0.0345					
0.0828	0.0	0.0	0.0	0.0242	0.1014				
0.0	0.0	0.0	0.0	0.0187	0.0	0.0			
0.0	0.0	0.0	0.0	0.0539	0.0	0.0834	0.1416		
0.0220	0.0	0.0	0.0	0.0	0.0	0.0	0.0	0.0	
0.0	0.0	0.0	0.0	0.0	0.0	0.0	0.0	0.0	0.0

Table 7.2: Estimates $\hat{\alpha}_i$ using $D800$ data.

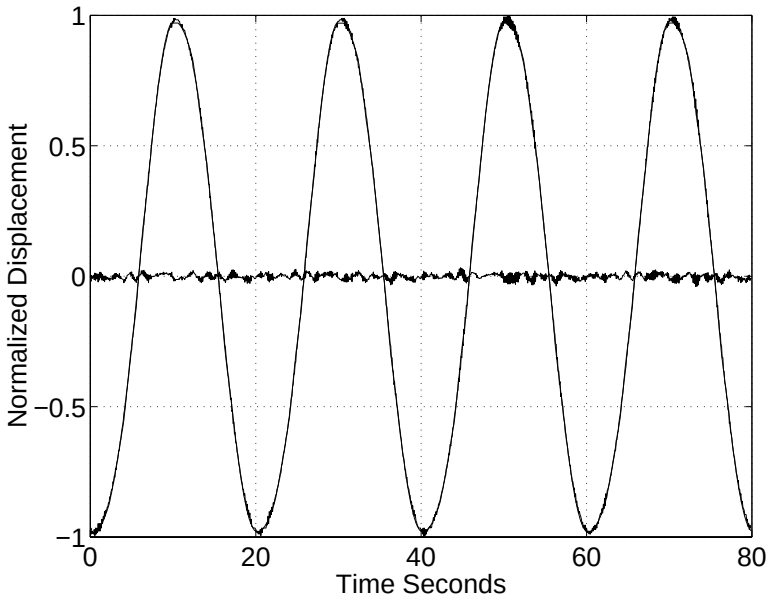

Figure 7.3: $\hat{w}$ estimate, w data and error for D800 data

7.3 Estimation of w using the Forward Operator $\mathbf{W}_n$

The accuracy of the approximation $\mathbf{W}_n$ was tested on an evaluation data set taken from the major and minor loops. This data was a different sample and not from the set used for identification. For each data set the input voltage u is used to estimate the displacement $\hat{w}$ with the formula,

$$\hat{w} = \mathbf{W}_n(u; \xi_{k-1}) = \sum_{i=1}^{n} \xi_u(\rho_i)\alpha_i$$

The data w, the estimates $\hat{w}$, and the error $e = \hat{w} - w$ are plotted for the test data set taken from D800, D600 and D400, in Figure 7.3, Figure 7.4, and Figure 7.5 respectively.

The model performed well in estimating the displacement w for all three data sets. The

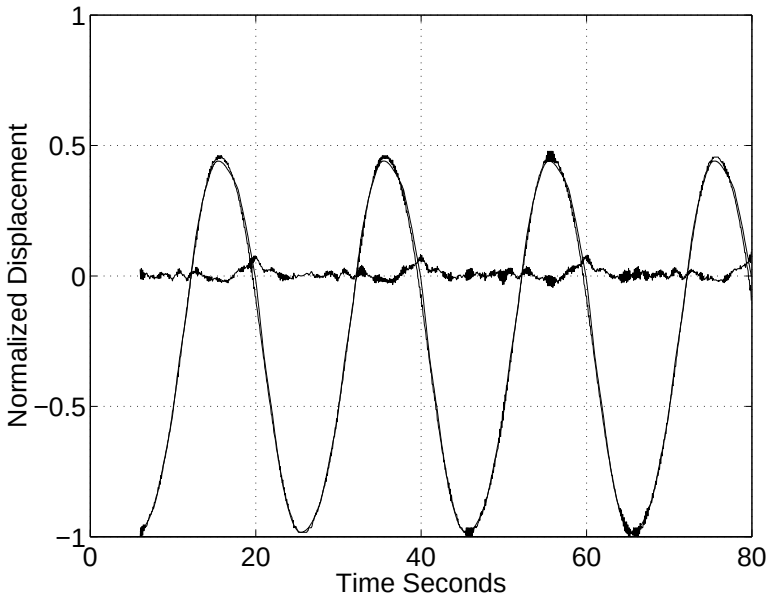

Figure 7.4: $\hat{w}$ estimate, w data and error for D600 data

Data	$max\|w - \hat{w}\|$
D800	0.0394
D600	0.093
D400	0.061

Table 7.3: Data Sets and estimation errors for $max|w - \hat{w}|$

maximum absolute error between the estimate and the normalized data for the D800 data is less than 0.0394. For the D600 data this error is less than 0.093, even though the inner loop data, D600, was not used for identifying the parameters α_i. Similarly for the D400 data, the absolute error on the normalized data is less than 0.061. Again, even though the D400 inner loop data was not used for estimating the parameters α_i, the model accurately estimates the displacement data. These results are summarized in Table 7.3.

7.4 Estimation of u^* using the Inverse Operator $\mathbf{W}_n^{-1}$

The input $u_n = \mathbf{W}_n^{-1}(w_d)$ was calculated using the algorithm described in Chapter 5. The performance of the inverse $\mathbf{W}_n^{-1}(w_d)$ was measured by the error between the experimental data u and the estimate u_n, $e = u - u_n$. The data u, the estimate u_n, and the error e are plotted for the data sets D800, D600 and D400 in Figure 7.6, Figure 7.7 and Figure 7.8.

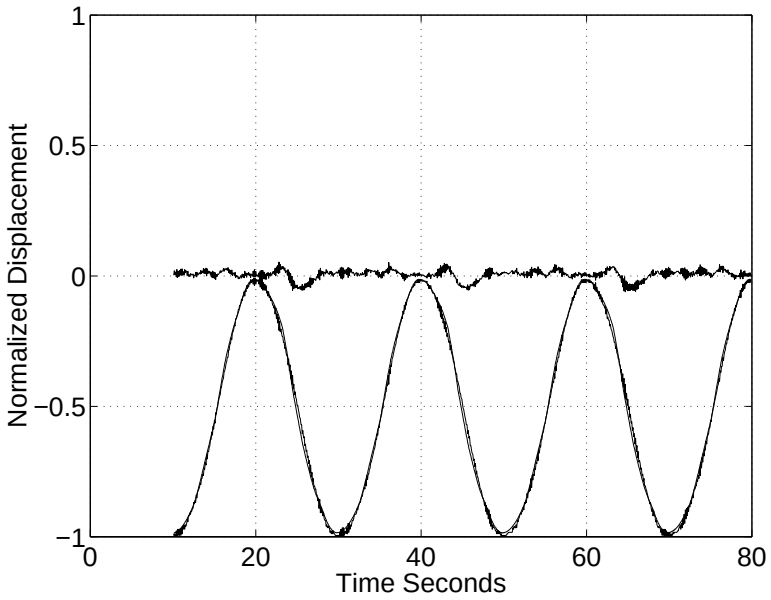

Figure 7.5: $\hat{w}$ estimate, w data and error for D400 data

Data	$max\|u - u_n\|$
D800	0.162
D600	0.179
D400	0.56

Table 7.4: Data Sets and estimation errors for compensated input u_n

The maximum absolute errors for each data set are given in Table 7.4. The maximum errors are 0.162 for the D800 data, 0.179 for the D600 data and 0.56 for the D400 data. The small errors indicate that the inverse is capable of estimating the input u fairly well even though only a portion of the major loop data was used in the parameter identification process and the discretization of the Preisach plane was not very fine.

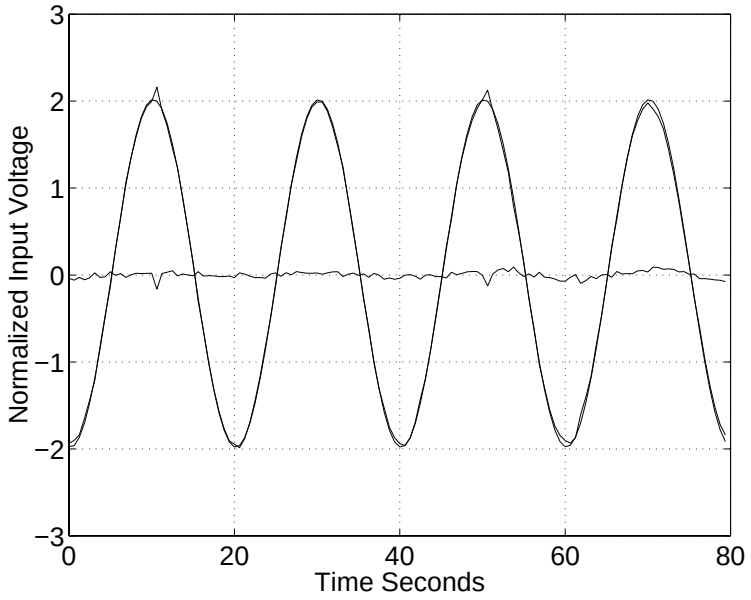

Figure 7.6: u , u_n and error for D800 data

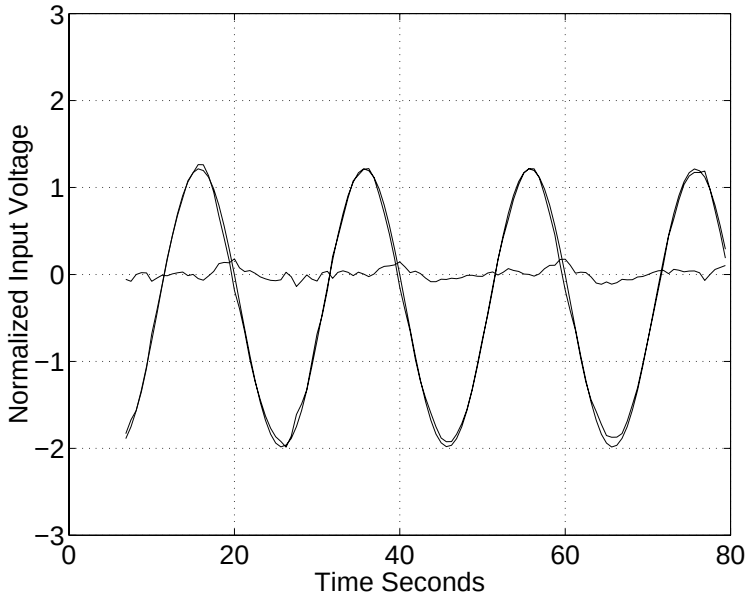

Figure 7.7: u, u_n and error for D600 data

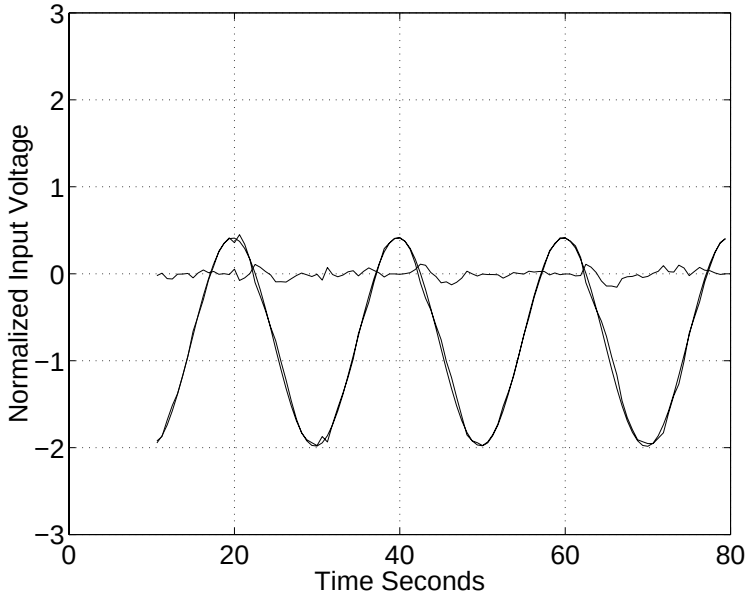

Figure 7.8: u, u_n and error for D400 data

Chapter 8

Concluding Remarks

Preisach type operators provide a versatile methodology for modeling scalar I/O hysteresis. It has been demonstrated that the classical Preisach and KP operators are capable of modeling certain types of hysteresis curves, and that each is invertible. An inverse was derived for each (for a single case for the Preisach) and used to demonstrate the feasibility of open loop control to minimize the effect of hysteresis.

The classical Preisach operator is based on a "relay" kernel and a weighting function (Preisach function) provided a priori. This parametric approach assumes a structure for the Preisach function $\nu(\rho)$ and has the advantage that it is necessary to identify only a small number of model parameters. However this comes at the cost of restricting the Preisach function to a single class of weighting functions. This restriction in turn limits the type of hysteresis curve that may be modeled by the operator. An additional problem with the Preisach operator is that, even though an inverse exists, it may not be possible to derive a function for the inverse. Therefore it may not possible to derive a computational form of the inverse, as required for the generation of the compensating input.

The KP operator is based on a connected kernel and not restricted to a particular measure. This property provides it with the potential to model a larger variety of hysteresis curves. The other strength of the KP model is that a computational form for the inverse exists for the given kernel. This advantage comes with the cost of requiring the identification of a large number of parameters, α_i. The hybrid system shown in Figure 8 is a compromise that is a synthesis of the strengths of both methods.

In the hybrid system the inverse of the discrete model generates a compensating input for the actuator. Position measurements from the actuator are then used to estimate the parameters of a weighting function $\nu(\rho)$. The discrete weights for the KP model are then derived from the weighting function, $\alpha_i = \int_{A_i} \nu(\rho_i) d\rho$ and updated in the discrete inverse. In this manner it may be possible to adaptively track the KP parameters with minimal computation and yet be assured of a compensating input.

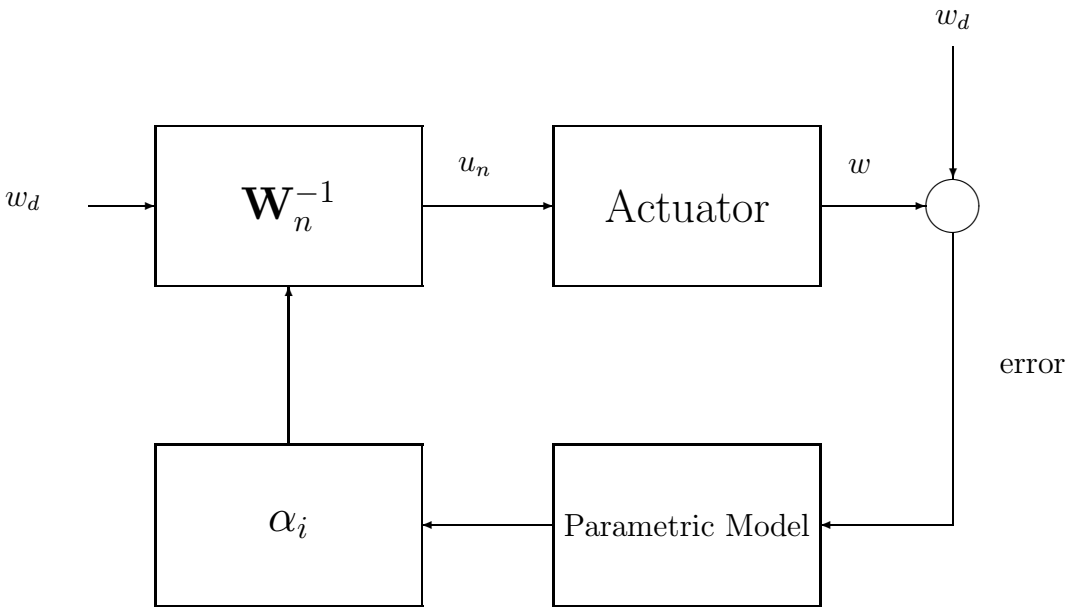

Figure 8.1: Hybrid System for Parameter Identification

Bibliography

[1] H. Banks, A. Kurdila, and G. Webb, "Identification of hysterestic control influence operators representing smart actuators part i:formulation," tech. rep., Center for Research in Scientific Computation, Department of Mathematics, North Carolina State University, Raleigh, NC 27695-8205 and the Department of Aerospace Engineering, Department of Mathematics, Texas A & M University, College Station, TX 77843, 1996.

[2] H. Banks, A. Kurdila, and G. Webb, "Identification of hysteretic control influence operators representing smart actuators: Convergent approximation," tech. rep., Center for Research in Scientific Computation, Department of Mathematics, North Carolina State University, Raleigh, NC 27695-8205 and the Department of Aerospace Engineering, Department of Mathematics, Texas A & M University, College Station, TX 77843, 1997.

[3] R. Gorbet, D. Wang, and K. Morris, "Preisach model identification of a two-wire sma actuator," in *International Conference on Robotics and Automation*, 1998.

[4] R. C. Smith, "A nonlinear physics-based optimal control method for magnetostrictive actuators," tech. rep., NASA, 1998.

[5] R. Smith, "A nonlinear model-based contol method for magnetostrictive actuators," in *Conference on Dec. and Control*, 1997.

[6] D. Lagoudas, Z. Bo, A. Kurdila, and G. Webb, "Micromechanics and control of hysteresis in shape memory alloys," in *Third ARO Workshop on Smart Structures*, 1997.

[7] J. Schäfer and H. Janocha, "Compensation of hysteresis in solid-state actuators," *Sensors and Actuators A* **49**, pp. 97–102, 1995.

[8] D. Hughes and J. T. Wen, "Preisach modeling and compensation for smart material hysteresis," *SPIE Active Materials and Smart Structures* **2427**, pp. 50–63, 1994.

[9] G. Tao and P. V. Kokotivić, "Adaptive control of plants with unknown hysteresis," *IEEE Transactions on Automatic Control* **40**, pp. 200–212, 1995.

[10] W. Galinaitis and R. Rogers, "Control of a hysteretic actuator using inverse hysteresis compensation," in *SPIE Smart Structures and Materials*, 1998.

[11] W. Galinaitis and R. Rogers, "Compensation for hysteresis using bivariate preisach models," in *SPIE Smart Structures and Materials*, 1997.

[12] G. Kádár, "On the preisach function of ferromagnetic hysteresis," *J. Appl. Phys.* **61**, pp. 4013–4015, 1987.

[13] E. Della Torre, "Existence of magnetization-dependent preisach models," *IEEE Transactions on Magnetics* **27**, pp. 3697–3699, 1991.

[14] F. Vajda and E. Della Torre, "Characteristics of magnetic media models," *IEEE Transactions on Magnetics* **28**, pp. 2611–2613, 1992.

[15] E. Della Torre and F. Vajda, "Parameter identification of the complete-moving-hysteresis model using major loop data," *IEEE Transactions on Magnetics* **30**, pp. 4987–5000, 1994.

[16] E. Della Torre, F. Vajda, M. Pardavi-Horvath, and C. J. Lodder, "Application of the variable variance hysteresis model to co-cr perpendicular recording media," *Journal of The Magnetics Society of Japan* **18**, pp. 117–120, 1994.

[17] A. A. Adly, I. Mayergoyz, and A. Bergqvist, "Preisach modeling of magnetostrictive hsyteresis," *J. Appl. Phys.* **69**, pp. 5777–5779, 1991.

[18] I. D. Mayergoyz, *Mathematical Models of Hysteresis*, Springer Verlag, 1991.

[19] M. A. Kransnosel'skiı and A. V. Pokrovskiı, *Systems with Hysteresis*, Springer Verlag, 1989.

[20] A. Visintin, *Differential Models of Hysteresis*, Springer Verlag, 1994.

[21] M. Brokate and J. Sprekels, *Hysteresis and Phase Transitions*, Springer Verlag, 1996.

[22] G. Bertotti, *Hysteresis in Magnetism: For Physicists, Material Scientists, and Engineers*, Academic Press, 1998.

[23] E. Della Torre, J. Oti, and G. Kadar, "Preisach modeling and reversible magnetization," *IEEE Transactions on Magnetics* **26**, pp. 3052–3058, 1990.

[24] E. Della Torre and F. Vajda, "The identification of the switching field distribution components," tech. rep., Institute for Magnetic Research, 1995.

[25] J. Oti, F. Vajda, and E. Della Torre, "Identification of parameters in a moving model," *J. Appl. Phys.* **69**, pp. 4826–4828, 1991.

[26] H. Bauer, *Probability Theory and Elements of Measure Theory. 2nd edition*, Academic Press, Inc., 111 Fifth Avenue, New York, NY 10003, 1981.

Chapter 9

Vita

Education:

1999 PhD in Mathematics
Virginia Polytechnic Institute and State University, Blacksburg, VA

1993 MA in Mathematics (Statistics emphasis)
Central Connecticut State University, New Britain, CT

1982 BS in Physics
The American University, Washington, DC

Work Experience:

1999 Ferrum College, Ferrum, Virginia
Assistant Professor, Mathematics and Statistics

1994-1998 Virginia Polytechnic Institute and State University, Blacksburg, VA
Mathematics Department, Graduate Teaching Assistant

1988-1994 United Technologies Research Center, East Hartford, CT
Associate Analytical Engineer

1987-1988 TRW, McLean, VA
Assistant Analytical Engineer

1983-1987 United Technologies Research Center, East Hartford, CT
Assistant Analytical Engineer

1982-1983 ADAPTRONICS INC., McLean, VA
Programmer

1978-1982 Atlantic Research Corporation, Alexandria, VA
Programmer

Publications:

Control of a Hysteretic Actuator using Inverse Hysteresis Compensation, W.S. Galinaitis and R.C. Rogers, SPIE Smart Structures and Materials, 1998, San Diego, CA

Compensation for Hysteresis using Bivariate Preisach Models, W.S. Galinaitis and R.C. Rogers, SPIE Smart Structures and Materials, 1997 San Diego, CA

Health Monitoring System for SSME- Fault Detection Algorithms, S. Tupule and W.S. Galinaitis, AIAA 26th Joint Propulsion Conference, 1990, Orlando, FL

Acoustic Emission Monitoring of SSME-ATD Roller Bearings, M. Hawman and W.S. Galinaitis, AIAA/ASME 25th Joint Propulsion Conference, 1989, Monterey, CA

Presentations:

Control of a Hysteretic Actuator using Inverse Hysteresis Compensation - ASME Mechanics and Materials Conference, 1999, Blacksburg, VA

Control of a Hysteretic Actuator using Inverse Hysteresis Compensation, SPIE Smart Structures and Materials, 1998, San Diego, CA

Compensation for Hysteresis using KP Integral Operator, 3rd ARO Workshop on Smart Structures, 1997, Blacksburg, VA

Compensation for Hysteresis using Bivariate Preisach Models, SIAM-SEAS, 1997, Raleigh, NC (Awarded best paper in section)